# CARBON NANOTUBES AND THEIR APPLICATION TO VERY LONG SPAN BRIDGES

by

Stéphane Damolini

French Engineer Degree
Ecole Spéciale des Travaux Publics, Paris
Class of 2009

Submitted to the Department of Civil and Environmental Engineering
in Partial Fulfillment of the Requirements for the Degree of

Master of Engineering

in Civil and Environmental Engineering at the

Massachusetts Institute of Technology   **ARCHIVES**

June 2009

Signature of Author: _____

Department of Civil and Environmental Engineering
May 8, 2009

Certified by: _____

Jerome J. Connor
Professor of Civil and Environmental Engineering
Thesis Supervisor

Accepted by: _____

Daniele Veneziano
Professor of Civil and Environmental Engineering
Chairman, Departmental Committee for Graduate Students

CARBON NANOTUBES AND THEIR APPLICATION TO VERY LONG SPAN BRIDGES

by

Stéphane Damolini

Spanning long distances in bridge construction relies mainly on the structure's efficiency and materials used. Whereas structural design for high rise building is fast-expanding, the overall design of long span bridges has not progressed significantly, and the increase in span chiefly depends of new materials.

Carbon nanotubes, with their extraordinary Young's modulus and tensile strength far exceeding steel, allow the production of ultra-strong cables which can be used for cable-based structures like suspension bridges. However, since nanoscopic elements are used to produce kilometer-long cables, it is difficult to calculate their real strength, taking into account physical and production defects.

This thesis provides the background necessary to understand the complexities involved in creating a kilometer-long cable made of carbon nanotubes. It also presents a computer program that computes the theoretical tensile strength of such a cable for a given set of assumptions about nanotubes. Scenarios varying the mechanical properties (tensile strength and Young's modulus) are applied to a cable-stayed and a suspension bridge, and it is shown than spans longer than five kilometers could be realized with such technology.

Thesis supervisor: Jerome J. Connor
Title: Professor of Civil and Environmental Engineering

Acknowledgments

I am grateful to everyone who made this thesis and degree possible:

my advisor, Professor Connor, for his knowledge and all his human qualities;

the Ecole Spéciale des Travaux Publics, for having supported my application to MIT;

my mom, for her kindness and her love;

my dad, for his advice and for always urging me to do more;

all of my friends, particularly Lana, Sabrina, Mehdi, and Olivier, with whom I had the best times;

last, but not least, Flavia and FX, for their great contribution to this unforgettable year.

Table of Contents

List of Figures

List of Tables

Introduction

Discovered in 1991 by Iijima [1], carbon nanotubes have been widely studied by an impressive number of researchers in the past decade. Indeed, these new forms of carbon have exceptional properties, not only mechanical, but also electrical, optical, chemical, thermal and biological, making their scope of use virtually unlimited. Shortly after their discovery, it was shown that these nanotubes have a Young's modulus that is several times that of diamond [2; 3]. In 1997, studies proved theoretically [4] and experimentally [5] that carbon nanotubes can withstand tremendous bending deformations within the elastic range. In 2000, Yu *et al.* [6] measured tensile strengths up to 63 GPa, a value 100 times greater than steel. In addition, their low density of 1.3 g/cm^3 [7] makes them the material with the highest specific strength in the world, up to 48,000 kN.m/kg.

With such properties and their extremely slender geometry, carbon nanotubes have become the perfect candidates for high performance wires or cables. However, aligning carbon nanotubes to form a wire results in a considerable loss in stiffness and tensile strength. For example, Li *et al.* [8] found the tensile strength of 20-mm long ropes to be approximately 3.6 GPa, a value still very high, but significantly smaller than the strength of an isolated nanotube. Therefore, evaluating the strength of a km-long cable made of nanotubes is a major problem. There are two options: produce a cable and test it, or evaluate the strength using mathematic analysis. Since cables exceeding a diameter of one centimeter have not been created yet, a mathematic analysis is required to obtain an order of magnitude estimate for the cable properties.

In this thesis, the first chapter is devoted to carbon nanotubes: their discovery, properties, and synthesis. The second chapter tackles the problem of estimating the tensile strength of cable made of nanotubes. Both experimental and mathematical results are presented, as well as a MATLAB® program that computes the strength of a kilometer-long cable made of nanotubes, using a multiscale stochastic simulation [9]. In the last chapter, different mechanical property scenarios are used to estimate reachable spans of cable bridges, particularly suspension-bridges, which take full advantage of these new high-performance cables.

1 Chapter One: The Material Carbon Nanotube
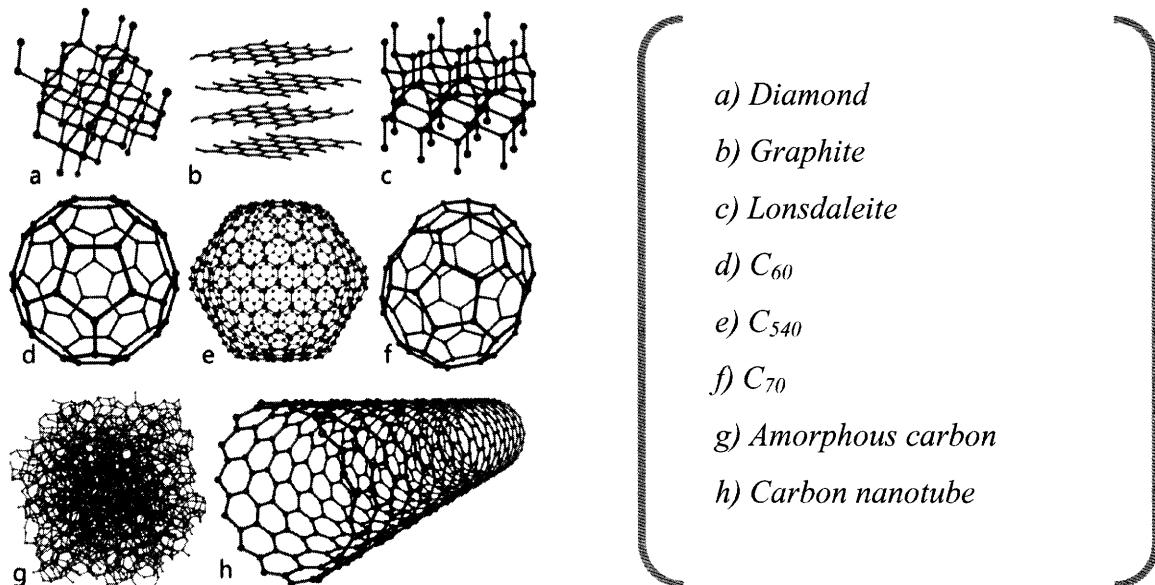
1.1 A New Carbon Family: Fullerenes.

Until the eighties, only three families of carbon were known: diamond, graphite, and amorphous carbon.

In the past decades, a new family has been discovered: fullerenes. Conceptually, fullerenes are molecules composed uniquely of carbon in the form of a hollow sphere, ellipsoid, tube, or plane. Fullerene was given its name in honor of the American R. Buckminster Fuller, who designed geodesic domes with similar topologies [10].

A Buckyball (also called C_{60}, or Buckminsterfullerene) is a particular arrangement of a spherical fullerene: it is the smallest molecule where two pentagons never share an edge [11]. It is constituted of 20 hexagons and 12 pentagons, for a total of 60 carbon atoms [12]. Bigger arrangements are named according to the number of carbon atoms: C_{72}, C_{76}, C_{84}, C_{100}, and so on.

When a fullerene takes the form of a tube[1], it is called a nanotube.

a) Diamond

b) Graphite

c) Lonsdaleite

d) C_{60}

e) C_{540}

f) C_{70}

g) Amorphous carbon

h) Carbon nanotube

Figure 1: The different carbon allotropes
(courtesy of Michael Ströck)

---
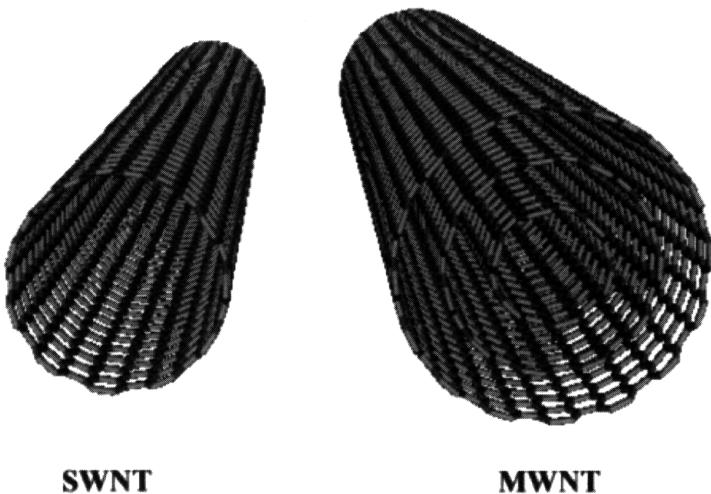
[1]Whereas fullerenes have been found in interstellar dust, carbon nanotubes are purely artificial, and have never been observed either in space or on Earth [13].

1.2 Carbon Nanotubes in Details

1.2.1 Definition
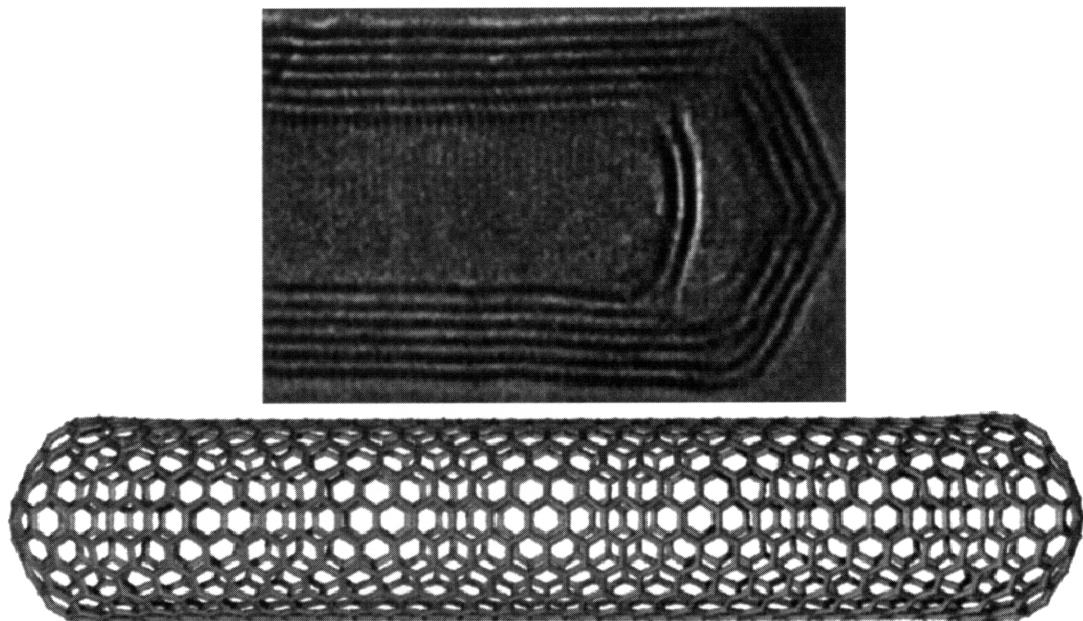
Basically, a carbon nanotube is a graphite sheet (i.e. carbon atoms arranged in hexagons) rolled into a cylinder of about 1 nanometer (1 nm = 10^{-6} m) diameter and up to several millimeters long. It can be geometrically visualized as a hair, but 100,000 times smaller.

In the hexagon shape, two consecutive carbon atoms are separated by 0.144 nm (vs. 0.142 in graphite), and two opposite atoms are separated by 0.283 nm.

SWNT   **MWNT**
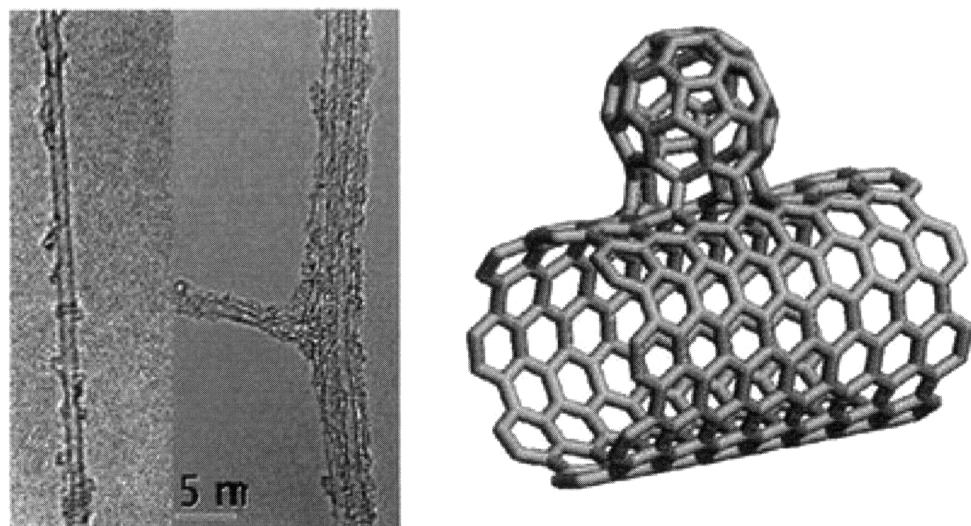
Figure 2: Two different types of nanotubes
(IBMC [52])

There are many different types of nanotubes. The most common distinction is on the number of layers, so called "walls." When a nanotube is made of one layer of graphite, it is called a Single-Wall Nanotube (SWNT), and when it is made of two or more concentric layers (up to over a hundred), it is called a Multi-Wall Nanotube (MWNT) (Figure 2). In this case, the diameter of the outer tube can reach tens of nanometers, with spacing between the different layers of typically 0.34 nm (3% greater than the spacing between sheets of graphite) [13]. In some cases, nanotubes are closed at their tip by a semi-sphere analogous to a half-Buckyball with at least six pentagons (Figure 3), or, have Buckyballs coming on their side (Figure 4).

9

Figure 3: A high resolution image of a MWNT (top), a model of a SWNT which is closed at its tips (bottom)
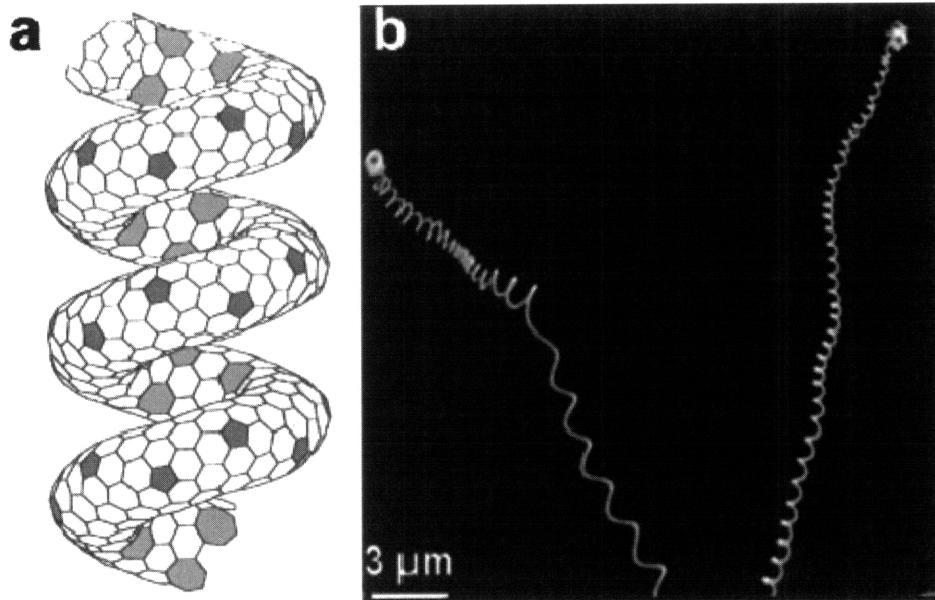
(adapted from P.M. Ajayanm [14])

Figure 4: Two TEM images of nanotubes with fullerenes attached to their surface (left), a model of a hybrid nanotube (with C_{60} attached) (right)

(Esko Kauppinen et al. [53])

Generally, the introduction of pentagons in a graphite sheet induces a (positive) curvature whereas heptagons induce a negative curvature [14] (that is to say, the top of the curvature is oriented toward the center of the tube). Consequently, numerous forms of nanotubes can be artificially made like helical SWNTs (Figure 5a) or corkscrew-like SWNTs (Figure 5b).
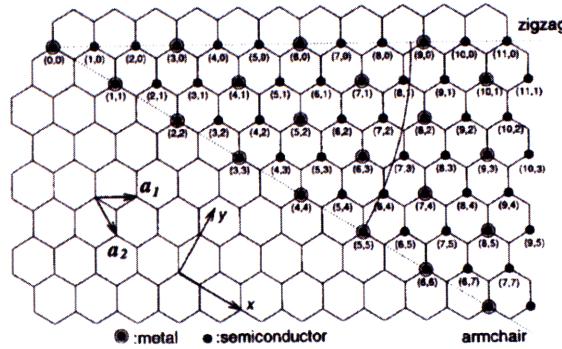
Figure 5: Helicoidal SWNT (a), corkscrew-like SWNT (b)
(N. Grobert [21])

Whereas graphite is a crumbly material (this property is used in pencils), nanotubes are very strong because carbon atoms are coiled [15]. Nonetheless, their properties depend on how the hexagons of carbon are geometrically arranged with respect to the axis of the tube: the chirality.

1.2.2 The Chirality
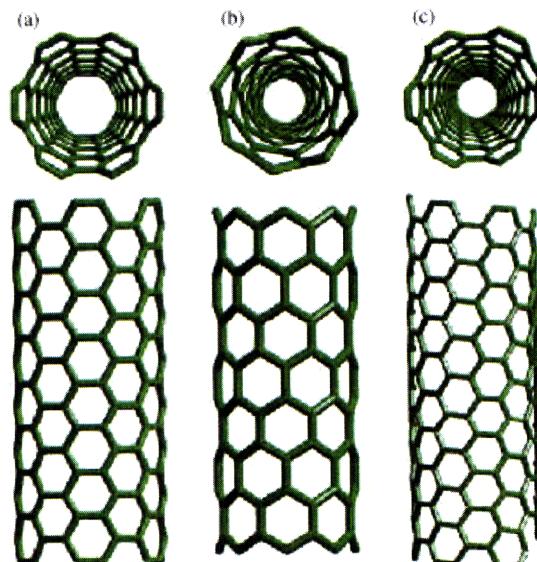
The way the graphene sheet is wrapped is represented by a pair of integers (n,m), determining the "chiral vector" (Figure 6) [14]: $C_n = ma_1 + na_2$.

Figure 6: The chiral vector of a nanotube

(M. S. Dresselhaus [54])

There are two particular configurations: when two opposite edges of a hexagon are perpendicular to the axis of the tube, the nanotube is called "armchair" (Figure 7 (a)); when two opposite edges of a hexagon are aligned with the axis of the tube, the nanotube is called "zigzag" (b). In any other configuration, the nanotube is called "chiral" (c) [14]. From these different arrangements, the characteristics of the nanotube vary. For instance, the fact that the nanotube is either metallic or semiconductor depends on the chirality, as shown in Figure 6.
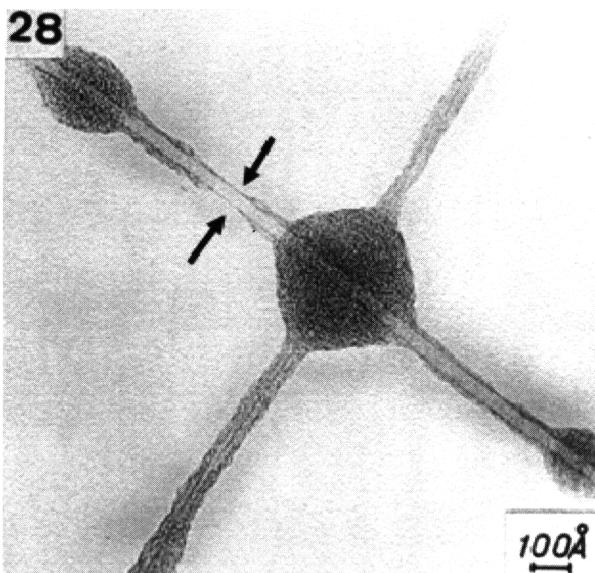
Figure 7: Chirality of nanotubes

(MRSEC [55])

12

1.3 Discovery

In 1952, L. V. Radushkevich and V. M. Lukyanovich in the *Journal of Physical Chemistry* [16] published the first images of MWNTs. Since the article was written in Russian and during the Cold War, this discovery was unnoticed by the scientific community [17].

In 1976, a picture likely representing a SWNT was shown (Figure 8); even though the authors did not give it a name [17; 18].
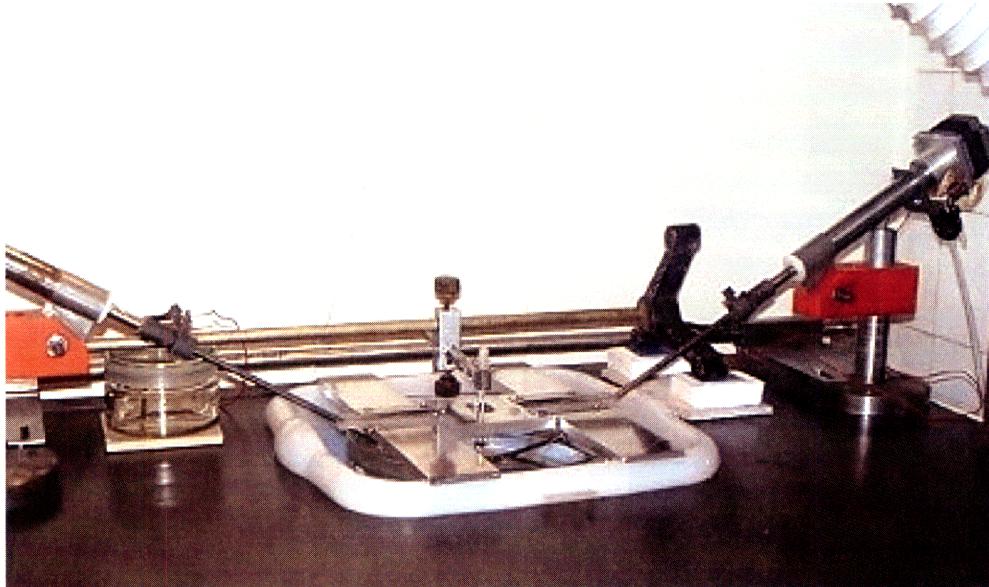
Figure 8: TEM image of what could be a SWNT
(Oberlin et al. [18])

However, the discovery of carbon nanotubes is attributed by a large number of scientists to Sumio Iijima, a senior research fellow at NEC corporation [1]. The discovery process started in 1971, when he developed the world's first high-resolution electron microscope at Arizona State University. When studying different carbon forms, he announced in 1980 that he saw "spherical graphite" of 1 nm of diameter, but he focused on the needle-shaped materials that were around it. After having hesitated between "microtubules," "tubulin," "NEC tubes," and "Iijima tubes," he finally chose the word "nanotubes", a word that would be easily recognized worldwide.

1.4 Synthesis

Carbon nanotubes can be obtained using different methods. The following sections detail the three main means of production, which have all their advantages and disadvantages.

1.4.1 Arc Discharge
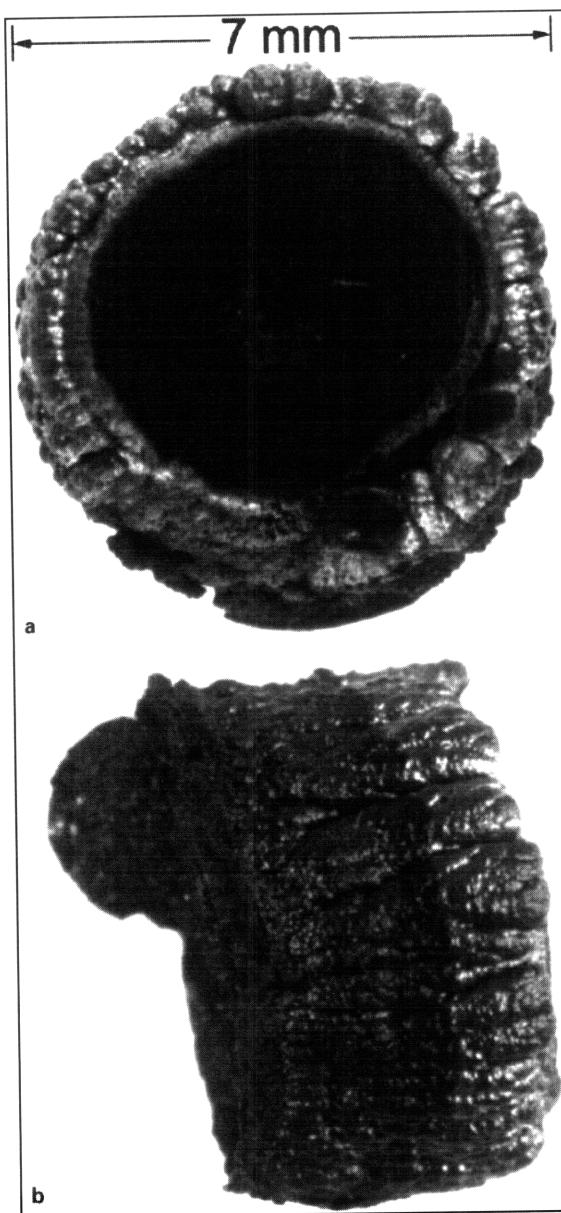
Figure 9: Arc discharge nanotube growth
(Research Institute for Technical Physics and Materials Science [56])

Initially used to produce fullerenes, the arc discharge method is the easiest and most common method to produce nanotubes [19] (Figure 9).

Typically, a direct current of ~90A is established between two high purity graphite electrodes (6-10 mm outside diameter) separated by 1 or 2 mm, and under a potential difference of approximately 20V. It has to be done in an inert gas environment (typically helium) at a low pressure (~600 hPa). During the discharge, the anode (positive electrode) is consumed and a deposit forms at a rate of 1 mm/min on the cathode (negative electrode) [14].

Figure 10: Macro view of an electrod deposit

Figure 11: Micro view of an electrod deposit

(M. Terrones [14])

Figure 10 represents two close views of the cathode after deposition. In view (a) the inner core of the electrode, in black, and the hard outer shell, in grey, are seen. A side view of the deposit is seen in (b).

Figure 11 is composed of microscopic views of the deposit from a Scanning Electron Microscopy (SEM). Images (a) and (b) show bundles that are themselves composed of nanotubes randomly oriented (c) [14].
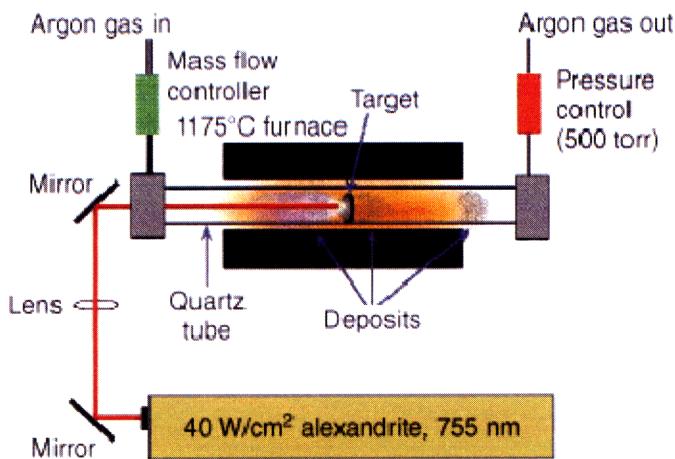
This method mainly produces MWNTs; however, modifying the parameters of the experiment (voltage, gas, electrodes, chamber geometry, cooling system, etc.) leads to different yields and nanotubes. In 1994, Journet *et al.* [20] obtained SWNT yields up to 90% using Nickel-Yttrium electrodes, a method which is now used worldwide.

The advantages of the arc discharge method are its simplicity, its relatively low cost, its yield (about 2 g/min using optimum settings [14]), and the high crystalline quality of the MWNTs [21].

The disadvantages of this method are that many carbon byproducts are produced, such as fullerenes, amorphous carbon and graphite sheets, and the nanotubes obtained are highly bundled and tangled [22]. Therefore, the purification costs are higher.

1.4.2 Laser Ablation

This method was pioneered by the Smalley Group in 1996 in their studies on fullerenes [23]. A pulsed laser vaporizes a graphite target in a high temperature furnace within an inert gas atmosphere. Typically, argon is used under a temperature of 1,200°C in order to produce MWNTs [14] (Figure 12).

Figure 12: Laser ablation diagram
(Laser Focus World [57])

However, to synthesize SWNTs, catalyst metal particles have to be used. Thess *et al.* [24] were the first to succeed in obtaining SWNTs, using graphite Co-Ni targets.

16

Recently, research has been done to produce nanotubes—particularly SWNTs—under a lower temperature. Kuo *et al.* [25] succeeded in producing MWNTs of 5-10 nm diameter at room temperature by using a high energy laser pulse (193 nm, 5 J/cm2 and 20 ns duration time). Zang and Iijima [26] performed laser ablation on fullerenes instead of graphite, and manage to synthesize SWNTs at a relatively low temperature of 400°C. Their results are shown in Table 1 (C_{60} refers to fullerene, M refers to the metal catalyst).

Table 1: Preparation conditions and TEM results for different samples

Sample No.	Target	Temperature (°C)	SWCNT formation
A	C_{60}+M	400	Yes
B	C_{60}	400	None
C	Graphite+M	400	Almost none
D	C_{60}+M	20	Almost none
E	C_{60}	20	None
F	Graphite+M	20	Almost none

(Zang and Iijima [26])

Like the other methods for producing nanotubes, varying the different parameters leads to different results. Regarding the laser, Heben *et al.*[27] showed the influence of its power: when the laser pulse power is increased, the diameter of tubes becomes narrower. Eklund *et al.*[28] demonstrated that ultrafast (less than one picosecond) laser pulses produce a large amount of SWNTs, at a rate of up to 1.5 g/h.

The advantage of this technique is the high purity of synthesized nanotubes [19]. Like the previous method, there are many byproducts, and the purification is difficult [29]. The yield, as in the arc discharge method, is approximately 70%. The main disadvantage of this method is its cost because high purity graphite rods and powerful lasers have to be used. Consequently, a large scale production is not imaginable [19].

1.4.3 Chemical Vapor Deposition

The chemical vapor deposition (CVD) method has been used for a century to produce carbon fibers [30].

In order to produce nanotubes, a substrate, a process gas, and a carbon-containing gas have to be used. The substrate is made with a layer of metal catalyst particles (iron, nickel, cobalt for instance); the process gas is typically ammonia, nitrogen or hydrogen; and the carbon-containing gas can be acetylene, ethylene, methane, etc.

The substrate is raised to 300-800°C (in order to obtain MWNTs) and up to 1,150°C (to obtain SWNTs) [21]. Then, the gases are blend into the reactor. When in contact with the catalyst molecules of the substrate, the carbon-containing gas breaks apart and the carbon atoms form nanotubes.
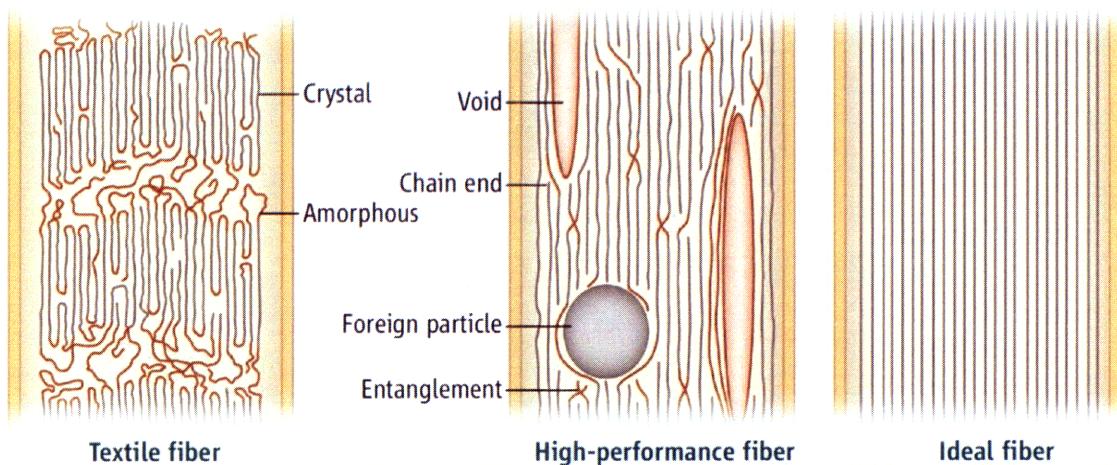
The advantage of this method is its versatility. All kinds of nanotubes can be produced: SWNTs and MWNTs, short and particularly long nanotubes, and also doped nanotubes—that is to say nanotubes on which a little amount of other atoms is added like boron and nitrogen, in order to modify their properties [31]. This method is the most promising for industrial production because it is inexpensive, the yields are high, aligned growth is possible, and the temperature used is relatively low. The disadvantages are the high quantities of silica, catalysts, and amorphous carbon byproducts, and it is more complex to obtain SWNTs [19].

Other methods exist like diffusion flame synthesis, electrolysis, solar energy based synthesis, heat treatment of a polymer, low-temperature solid pyrolysis, and ball milling. For the moment, these methods do not have an industrial future.

2 Chapter Two: A Cable Made of Nanotubes

2.1 About High-Performance Fibers

Kevlar, the first high performance fiber, was developed in 1965 by DuPont scientists [32]. In the 1980s, Spectra® and Dyneema® were the first fibers processed from polyethylene. In 1998, the high-strength polymeric fiber Zylon® was commercialized. Although extremely strong, the density of these fibers is relatively high [33].

Figure 13: Structure of various fibers
(Han Gi Chae & Satish Kumar[33])

Like any high-performance fiber, a carbon nanotube fiber has to have a limited number of imperfections to optimize its strength. These imperfections can be layout defaults of the nanotubes, such as chain ends or entanglements, or can be the presence of foreign particle or voids [34; 33]. As shown in Figure 13, these imperfections result in stress concentration in which a failure is more likely to happen, lowering the entire fiber tensile stress.

Concerning the nanotubes themselves, they have to meet certain requirements. Indeed, the first criterion is that a nanotube should have the best structure possible. A well structured nanotube has straight walls (no pentagons or heptagons), and no impurities. The best candidates for these requirements are SWNTs and 2WNTs (i.e., MWNTs that have only two walls) because they are the kinds of nanotubes that are the most defect-free during their synthesis [34]. In addition, they have a natural tendency to assemble in parallel into bundles. Even if MWNTs (with more than two walls) without defects were

obtained, they would be less effective because the small benefit in strength would be off-
set by the large increase in density. Because graphite is a lubricant, and the interaction
between graphite sheets is weak, the interaction between carbon nanotubes is weak.
Consequently, the contact surface between tubes has to be maximized to increase the
shear transfer. This is the same principle used in reinforced concrete, where the reinforc-
ing bars must overlap a certain length to transfer the force through concrete. With nano-
tubes, the transfer is done through Van der Waals forces. SWNTs and 2WNTs are suita-
ble as well because it has been observed [34] that they flatten against each other, and can
be grown with a length of the order of 1 mm and a diameter up to 10 nm, maximizing the
contact area. Another promising means to increase interaction has been introduced by
Kis *et al.* in 2004. In their paper [35], they use an electron-beam irradiation to create sta-
ble links between carbon nanotubes within bundles. The sliding between carbon nano-
tubes being eliminated, the bending modulus measured was 30 times higher.

2.2 The Binding and Aligning Processes

As discussed in 2.1, the binding process is critical in order to maximize the transfer
of individual nanotube properties to the fiber. Until now, various techniques have been
used to spin nanotube fiber, all with their advantages and disadvantages. The ideal would
be to have an industrially viable technique, having a high yield, and giving a fiber with
high and constant properties. Carbon nanotubes can either be produced by any method
discussed in 1.3, suspended, then spun into a fiber; or they can be directly spun as soon as
they are synthesized. The first process could involve, for example, a spinning from a lyo-
tropic liquid crystalline suspension of nanotube, which results in rather stiff but relatively
weak fibers [36; 34]. The second process could be, for instance, the direct spinning from
an aerogel of SWNTs and 2WNTs, as they are produced using a chemical vapor deposi-
tion [34]. The promising results are given in 2.3.2.

2.3 Mechanical Properties

2.3.1 Theoretical Values Based on Probability Analysis

In the following, the strength calculation of a km-long cable made of nanotubes is addressed. To do so, a MATLAB® code was written by the author, according to the theory developed by Nicola Pugno *et al.* [9].

2.3.1.1 The Model

The purpose is to start from the nanoscale strength of nanotubes, and reach a macroscale strength using statistics and extrapolation.

The **level 0** (nanoscale) consists of a single nanotube that was chosen to be 1-nm diameter, 100-nm length, and a given Young's modulus. The maximum tensile strength of this nanotube is randomly given, using a Weibull distribution [37]:

$$f(\sigma) = \frac{m}{\sigma_0}\left(\frac{\sigma}{\sigma_0}\right)^{m-1} e^{-\left(\frac{\sigma}{\sigma_0}\right)^m}$$

where f is the probability density function of a tensile strength σ, σ_0 is an experimental value, and *m* is the parameter of the distribution. It has been found [37] for SWNTs that $\sigma_0 = 34,000$ MPa and $m = 2.7$. The function f is drawn in Figure 14. To generate Weibull-distributed random variates, the following formula was used:

$$\sigma = \sigma_0(-\ln(u))^{\frac{1}{m}}$$

where σ is a Weibull-distributed tensile strength, and u is a random number in the interval [0; 1].
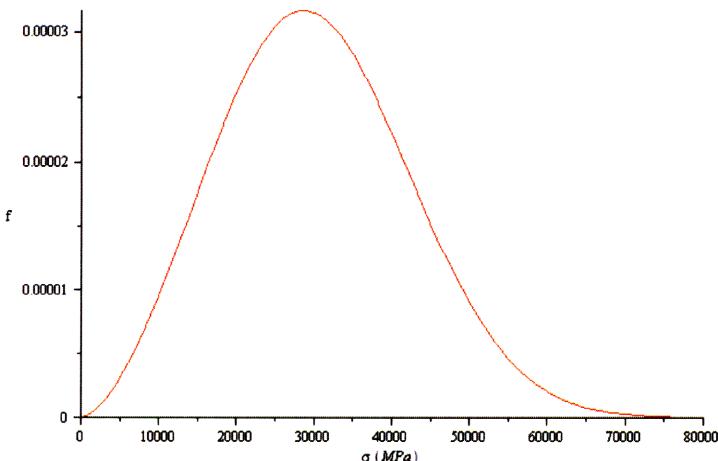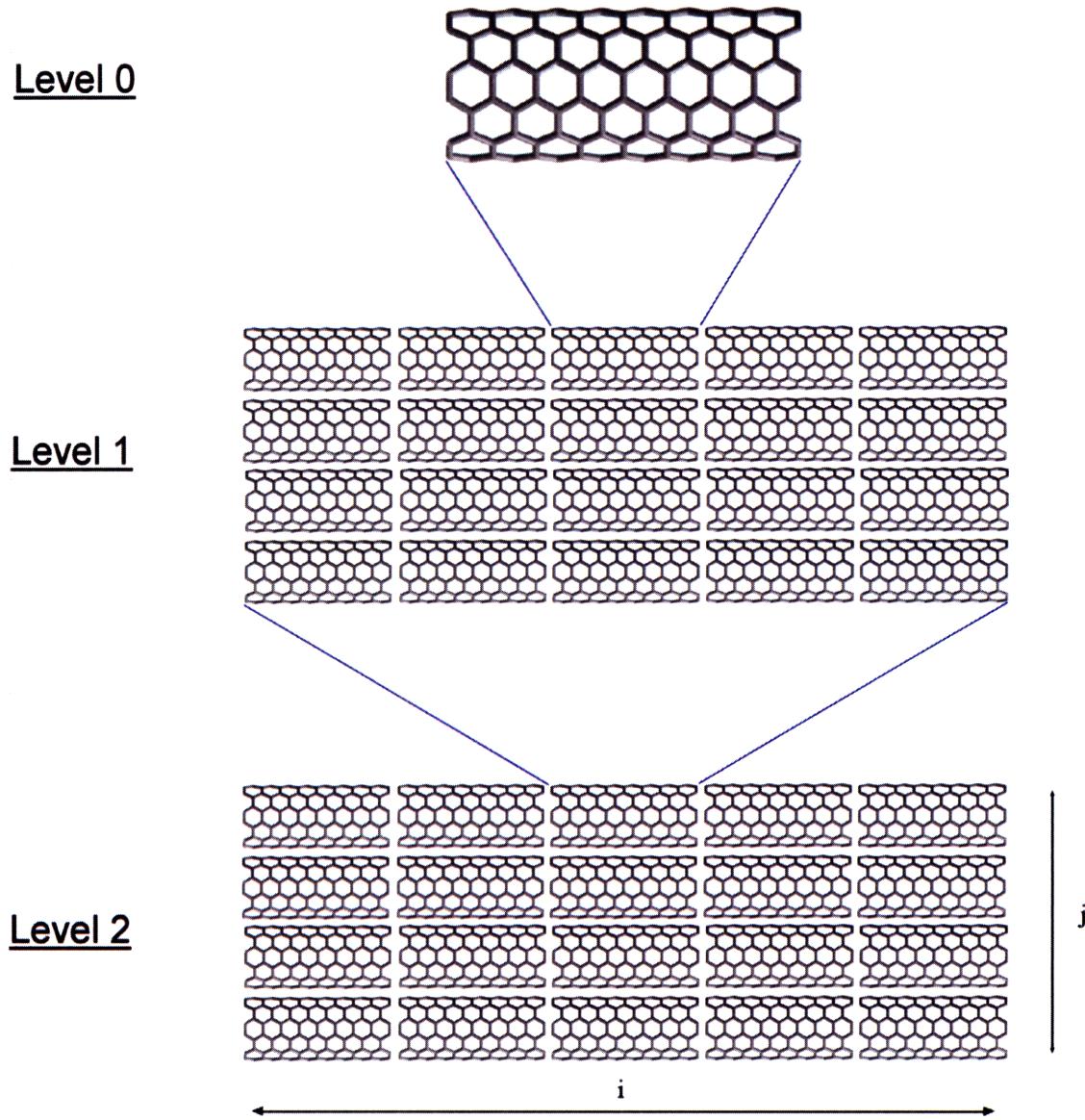
Figure 14: Probability density function of the Weibull distribution

21

Figure 15: Explanation of the different levels of iteration
(adapted from COECS [58])

The **level 1** consists of an array of nanotubes, arranged in parallel sections (Figure 15). Each nanotube comes from level 0 and has a given and random tensile strength. At this point, the program computes the strength of this given array of nanotubes. If fact, this array is represented by a matrix of i rows and j columns. In each entry, the strength of the nanotube is stored. The program simulates a tensile stress applied to the whole array, as if it were a single entity. When the stress reaches a value exceeding the limit of the weakest nanotube, this nanotube breaks, and its stress is uniformly redistributed

among the remaining nanotubes in the row (a row represents a cross section in the real strand or cable). Then, the program continues to increase the applied stress until a row is composed only of broken nanotubes. At this point, the "cable" fails and the maximum allowable stress of this given array is obtained.

The **level 2** is obtained in a similar way. Instead of being constituted of nanotubes, it is constituted of arrangements from level 1. Indeed, the base pattern is a new $i \times j$ matrix, where each entry is another $i \times j$ matrix coming from level 1. Consequently, a level 2 matrix is composed of $(i \times j)^2$ nanotubes.

To reduce the computing time, not every sub-matrix constituting the level 2 is computed. Instead, it is only computed a number *ns2* of level 1 matrices, and then a strength amongst this sample is randomly chosen by the program. The number *ns2* is chosen by the user. The higher the *ns2*, the greater the sampling, the better the results. It will be seen later how the sampling size impacts the calculation time.

The other levels are derived from the level above in the same fashion. When level n is reached, a "cable" consisting of $(i \times j)^n$ nanotubes is obtained: i^n in the length and j^n in a cross section. The assumptions made about the nanotubes dimensions (1-nm diameter, 100-nm length) led the author to choose $n = 7$, $i = 27$, and $j = 373$ to simulate a cable in the order of 1-km long, and 1-m diameter.

2.3.1.2 Parameters of the Program

The main parameters changeable by the user are:

s_0 The stress σ_0 used before in the Weibull statistic

k_0 The parameter of the Weibull statistic

ii   The length of a base pattern

jj   The width of a base pattern

Δs_0 The increment in tensile strength (*delta_s0* in the code)

nsi   The sampling size of level *i*-1 for level *i*.

The full code is provided in Appendix A.

2.3.1.3 Results and Discussion

The tensile strength of the kilometer long cable was computed with the program. The value obtained is **14,390 MPa**.

It was found that the higher the level of iteration, the lower the dispersion of tensile strengths. Consequently, the sampling size has been chosen to be very large for the first levels and lower for the other levels:
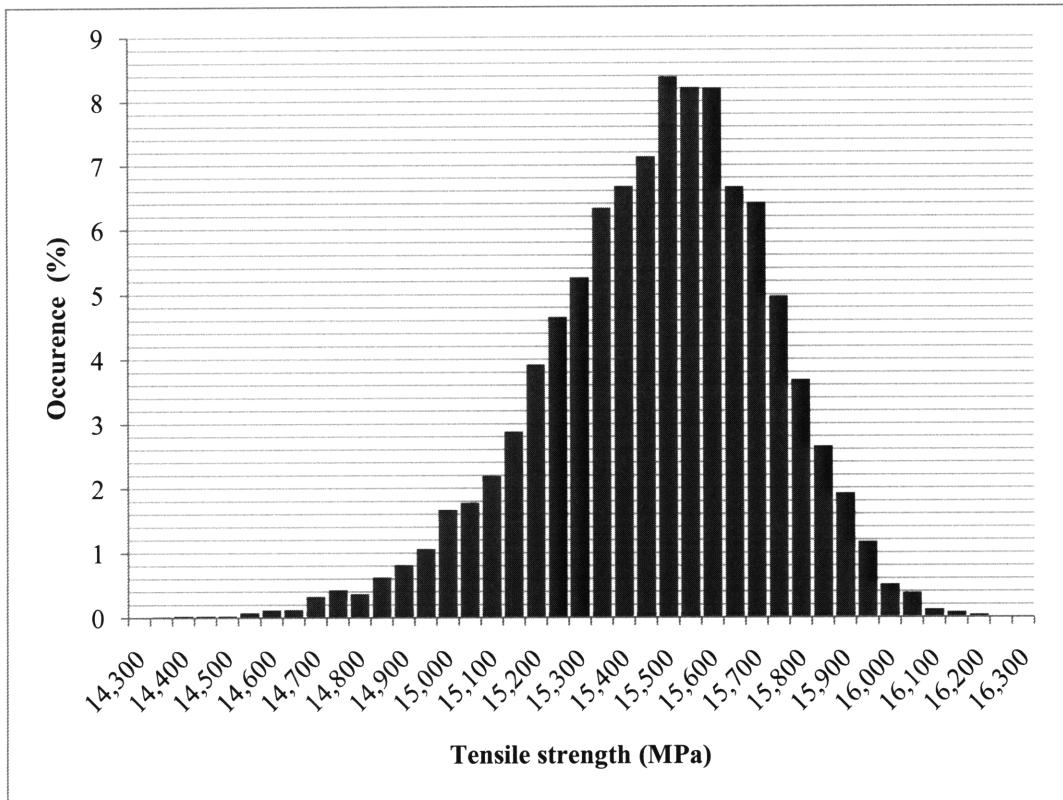
Level 1: 10,000 samples

Level 2: 1,000 samples

Level 3: 100 samples

Level 4: 10 samples

Level 5: 10 samples

Level 6: 5 samples

Level 7: 5 samples

Concerning Level 0, it was decided to not take samples of it but to compute the strength of all nanotubes according to Weibull statistics.
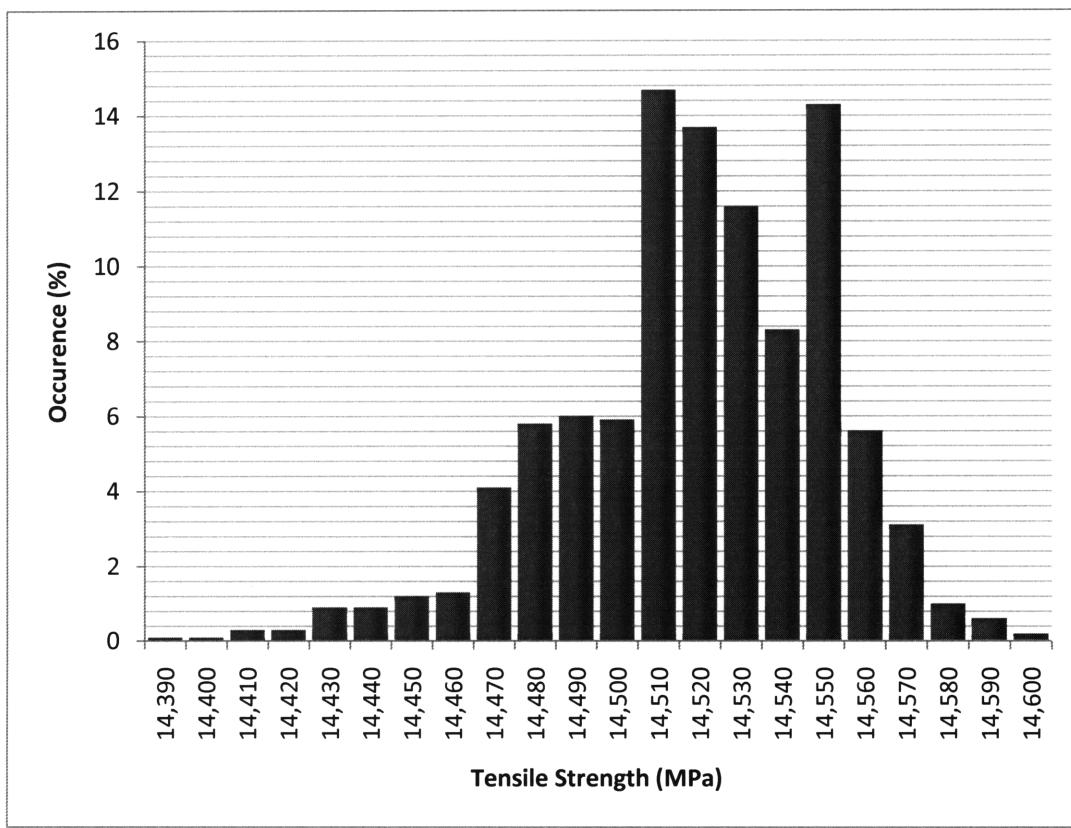
To enhance the accuracy, higher values of sampling can be used but the computation time will increase:

$$\text{computation time} \propto i \times j \times (1 + ns2 + ns3 + ns4 + ns5 + ns6 + ns7)$$

With Δs_0 set to 10 MPa (the tensile strength increment), and for the values given above, the computation time on a personal computer is about four hours. For SWNTs, the samplings of level 1 and level 2 are shown in Figure 16 and Figure 17. For Level 1, the distribution of the 10,000 samples is close to another Weibull distribution. Concerning level 2, the values are closer and smoothly distributed except for 14,500 and 14,550 MPa. At the higher levels, all the samples have the same tensile strength, the final one (14,390 MPa). However, using higher sampling sizes for level 1 and 2, and lowering Δs_0, will give multiple values for higher levels, but such accuracy is irrelevant, knowing the numerous assumptions that have been made.

Figure 16: Distribution of level 1 samples
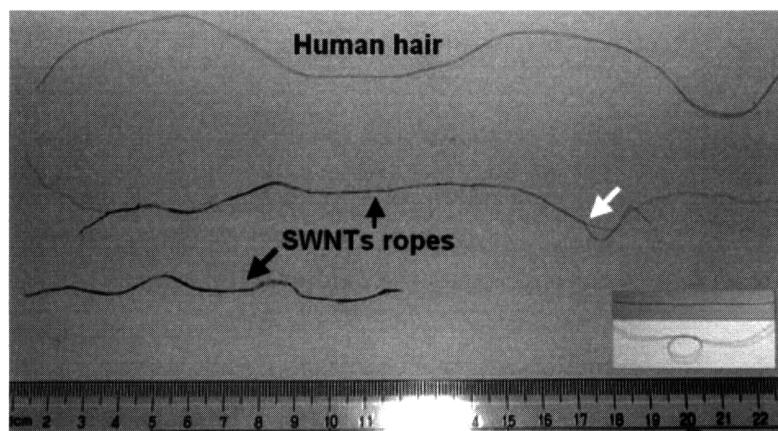
Figure 17: Distribution of level 2 samples

25

The order of magnitude of the tensile strength computed is consistent, but many assumptions were made. It was supposed that the link between vertical nanotubes was perfect, that the stress was instantly and uniformly distributed over all the cross section when a nanotube breaks, that all the nanotubes had the same dimensions, and that they had the same Young's modulus. Therefore, the value obtained is an optimistic upper bound of the value reachable in reality.

2.3.2 Experimental Values
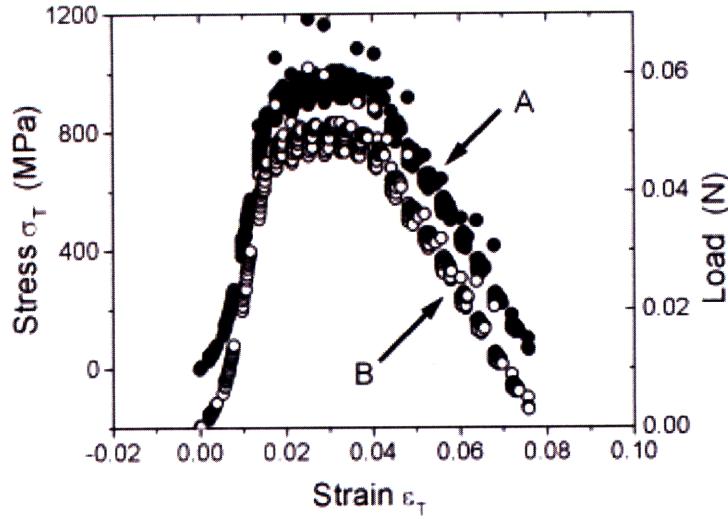
Experimental values vary greatly from one study to another because the operating procedures are not the same. Different means of synthesis are used with different techniques of spinning, leading to different sample sizes, the properties of which are measured with different devices, according to different mathematical models. Even the material properties are not always clearly defined. Some authors compute the Young's modulus and tensile strength using the effective section of nanotubes (i.e., the section occupied by the ring composed by the carbon atoms) whereas others use the engineering section, including the empty space within the tube.

In 2002, Zhu *et al.* [38] produced nanotube strands using an optimized catalytic chemical vapor deposition technique. They reached length of up to 20 cm, as shown in Figure 18. Because of the macro scale of the ropes, they can be manipulated by hand and tested in a classic tensile test machine. Figure 19 (curve A) represents the true stress-true strain curve ("true" means that the section of the cable is actualized at every measurement). The authors obtained tensile strengths up to 1,200 MPa, and according to them,

Figure 18: Two cm-long nanotube ropes

(Zhu et al. [37])

26
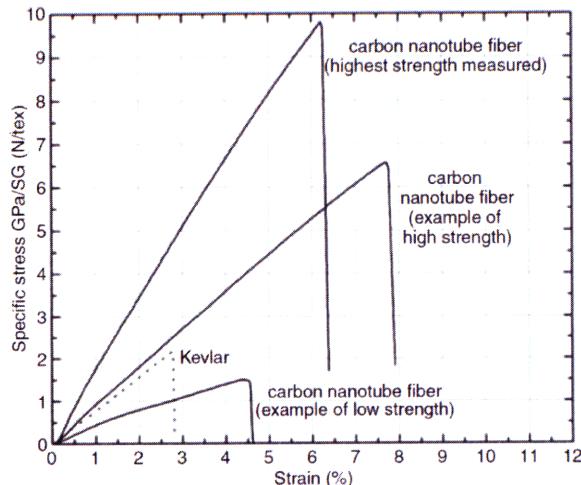
Figure 19: True stress - strain curve
(courtesy of Zhu et al. [37])
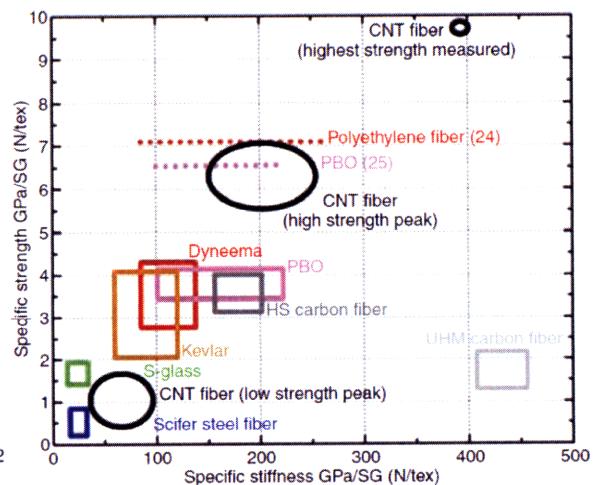
the bell shape of the curve is a consequence of the slippage between nanotubes (as seen in Section 2.1), which depicts a plastic deformation.

In 2007, Koziol *et al.* [34] measured the strength of a carbon nanotube fiber, spun directly from gas phase as an aerogel. For a 1-mm fiber, they obtained specific stresses of up to 9.7 GPa/SG (Figure 20) (the specific stress being the yield stress divided by the specific gravity (SG), the specific gravity being the density of the material divided by the density of water). Given the specific gravity of 0.9, a maximum tensile strength of approximately 9 GPa and a Young's modulus of approximately 350 GPa are derived. The results of this study are compared to other high-performance fibers (Figure 21).

Figure 20: Specific stress - strain for a carbon nanotube fiber

Figure 21: Different fiber performances

(Koziol et al. [34])

27

2.3.3 Conclusion About Mechanical Properties

There is a large variability in the results of all the studies. Neither experimental nor mathematic results are accurate, simply because any infinitesimal error on the nanoscale becomes significant on a centimeter or a kilometer scale.

To conclude Chapter Two, five different scenarios regarding the performance of a km-long cable made of nanotubes have been chosen by the author. They are presented in Table 2.

Table 2: Five scenarios of carbon nanotube cable mechanical properties

Scenario	Young's modulus (GPa)	Tensile Strength (MPa)
Pessimistic	250	2,000
High Stiffness	500	2,000
High Strength	250	10,000
Optimistic	500	10,000
Very Optimistic	1,000	20,000
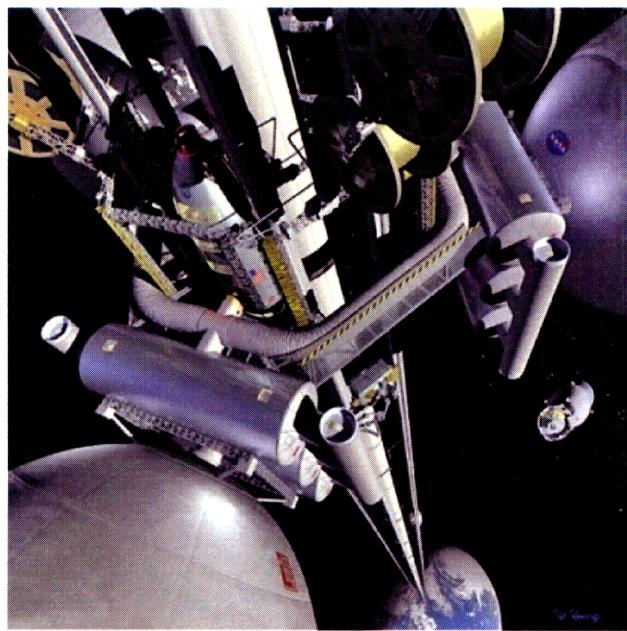
3 Chapter Three: Application to Bridges

3.1 About the Space Elevator

This chapter presents a bridge linking the Earth to space: the "space elevator."

Basically, a space elevator would consist of a climber sliding on a cable attached to the Earth at one end, and free in space at the other end, approximately 150,000 kilometers above the Earth's surface (Figure 22). To satisfy equilibrium, two opposite forces would be exerted on the cable: the gravitational force and the centrifugal force. Unlike gravity, which applies only within the atmosphere, the centrifugal force applies everywhere, and when the cable height reaches 150,000 kilometers, this force would overcome gravity and the cable would stand by itself [39].

If built, this space elevator would be used to carry payloads or even satellites into space, at a very low cost compared to that of launching rocket. However, the design of such an elevator is a huge challenge, and new high performance materials have to be utilized. The main problem is to design the cable on which tremendous forces will act. It has to be both extremely light and strong. Only a carbon nanotube cable might fulfill the stringent strength requirements.
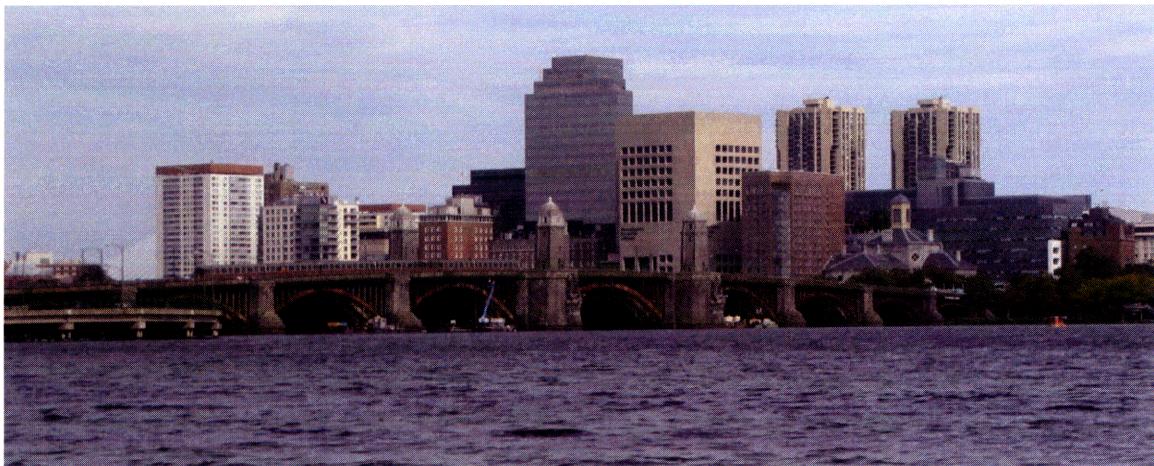
Figure 22: The Space Elevator
(Life Boat Foundation [59])

3.2 Cable-Stayed Bridges
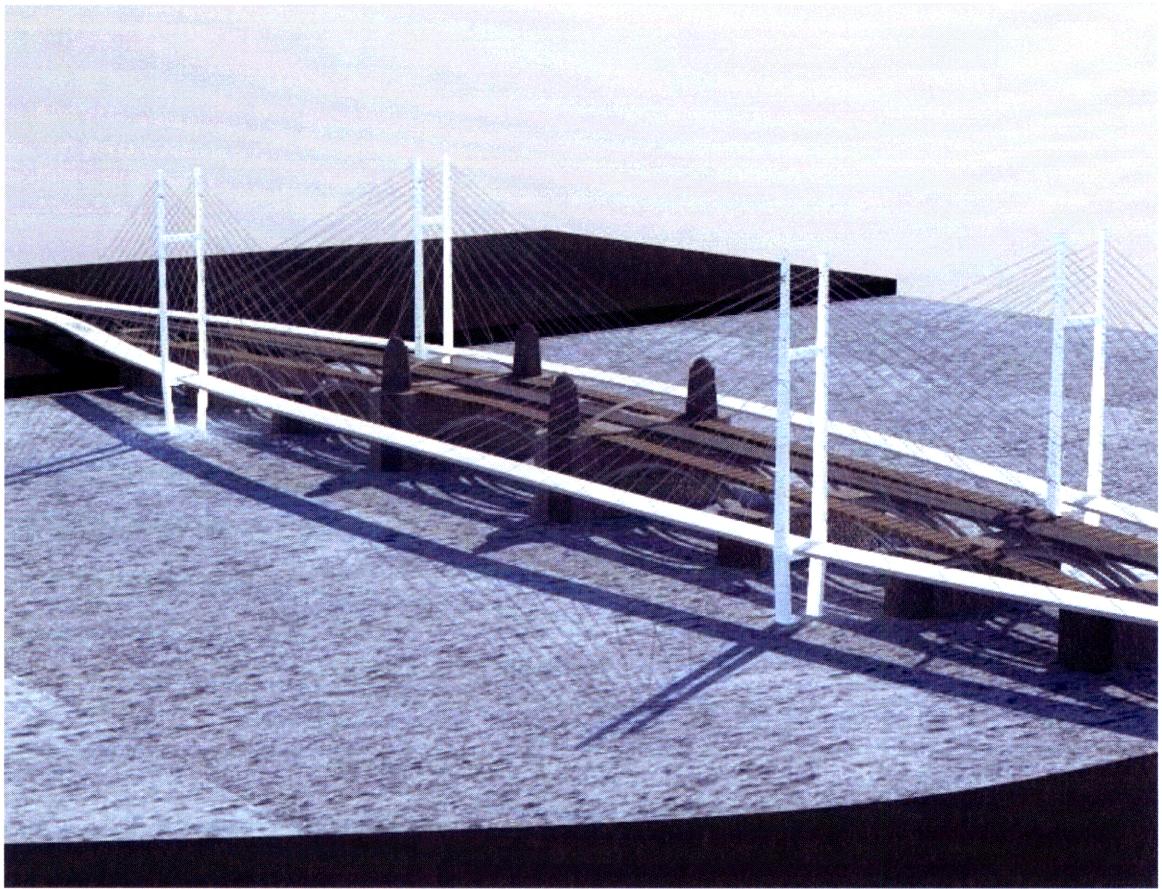
3.2.1 Case Study: the Longfellow Bridge Replacement

To determine the advantages of using a cable made of carbon nanotubes, the different scenarios given in Section 2.3.3 are applied to a cable-stayed bridge project. The Longfellow Bridge Replacement [40], a project done by Architectural Structures Network (ASN), a team composed of MIT students, is considered.

Figure 23: The Longfellow Bridge
(courtesy of S. Damolini)

The Longfellow Bridge crosses the Charles River, between Boston and Cambridge, Massachusetts (Figure 23). Completed in 1904, its structure is currently deficient, and there are strict traffic restrictions. Since it is a major link between the two cities, ASN designed two new bridges beside the existing one, which will be turned into a pedestrian area. They are two identical cable-stayed bridges, with two back spans of 128 m, and a main span of 256 m (Figure 24).

Figure 24: The final alternative proposed by the ASN team
(courtesy of ASN [40])

The cable sections for half of the main span were computed using the different cable properties (Young's modulus and tensile strength) assumed in the various scenarios. Both a Strength Based Design (SBD) and a Motion Based Design (MBD) [41] were used. The former aims to satisfy the strength requirement of the cables, and it is mainly dependent on the tensile strength, whereas the latter aims to satisfy the maximum vertical displacement requirements of the deck, and it is mainly dependant on the Young's modulus. For every cable, both sections are computed, the greater is selected and then multiplied by a safety factor (2.5 in this case).

Calculation details are given in Appendix B, and results are given in the following section.
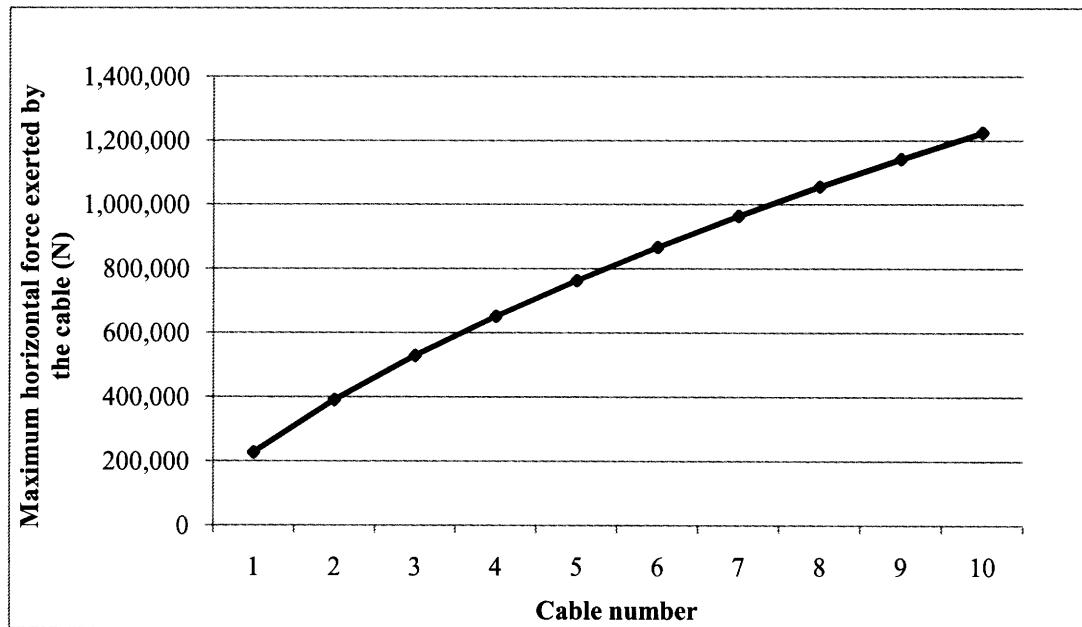
3.2.2 Results and Discussion

As shown in Table 3, substantial reductions in the cable sections are obtained using high-performance fibers. Generally, the sections for the shortest cables are determined by Strength Based Design, and the sections for the longest cables by Motion Based Design. Consequently, an increase in stiffness has no impact on the short cables, whereas an increase in the tensile strength has no impact on the long cables. For example, the sections are identical for the first four cables in the "pessimistic" and "high stiffness" scenarios, and for the last six cables of the "pessimistic" and "high strength" scenarios.

Table 3: Cable sections with the different scenarios

Scenarios	Cable #	1	2	3	4	5	6	7	8	9	10
	Horizontal distance (m)	12.19	24.38	36.58	48.77	60.96	73.15	85.34	97.54	109.73	121.92
Reference E = 200 GPa σ = 1.5 GPa	Cable diameter (cm)	3.51	3.75	3.99	4.23	4.74	5.57	6.42	7.31	8.22	9.17
	Section size driven by	Strength	Strength	Strength	Strength	Disp.	Disp.	Disp.	Disp.	Disp.	Disp.
Pessimistic E = 250 GPa σ = 2 GPa	Cable diameter (cm)	3.04	3.24	3.46	3.66	4.24	4.98	5.74	6.53	7.34	8.17
	Section size driven by	Strength	Strength	Strength	Strength	Disp.	Disp.	Disp.	Disp.	Disp.	Disp.
	Reduction in section	13.4%	13.4%	13.4%	13.4%	10.6%	10.6%	10.6%	10.6%	10.7%	10.9%
High Stiffness E = 500 GPa σ = 2 GPa	Cable diameter (cm)	3.04	3.24	3.46	3.66	3.85	4.03	4.19	4.61	5.18	5.76
	Section size driven by	Strength	Strength	Strength	Strength	Strength	Strength	Strength	Disp.	Disp.	Disp.
	Reduction in section	13.4%	13.4%	13.4%	13.4%	18.7%	27.7%	34.8%	36.9%	37.0%	37.2%
High Strength E = 250 GPa σ = 10 GPa	Cable diameter (cm)	1.71	2.24	2.86	3.53	4.24	4.98	5.74	6.53	7.34	8.17
	Section size driven by	Disp.	Disp.	Disp.	Disp.	Disp.	Disp.	Disp.	Disp.	Disp.	Disp.
	Reduction in section	51.3%	40.2%	28.4%	16.6%	10.6%	10.6%	10.6%	10.6%	10.7%	10.9%
Optimistic E = 500 GPa σ = 10 GPa	Cable diameter (cm)	1.36	1.59	2.02	2.49	3.00	3.52	4.06	4.61	5.18	5.76
	Section size driven by	Strength	Disp.	Disp.	Disp.	Disp.	Disp.	Disp.	Disp.	Disp.	Disp.
	Reduction in section	61.3%	57.7%	49.4%	41.0%	36.8%	36.8%	36.8%	36.9%	37.0%	37.2%
Very Optimistic E = 1,000 GPa σ = 20 GPa	Cable diameter (cm)	1.36	1.45	1.55	1.76	2.12	2.49	2.87	3.26	3.66	4.07
	Section size driven by	Strength	Strength	Strength	Disp.	Disp.	Disp.	Disp.	Disp.	Disp.	Disp.
	Reduction in section	61.3%	61.3%	61.3%	58.3%	55.3%	55.3%	55.3%	55.4%	55.5%	55.7%

Therefore, spanning long distances with a cable-stayed bridge requires mainly high cable stiffness. However, cables are not the limiting factor for this type of bridge. As the span increases, the compression on the deck becomes very important. The horizontal force exerted by one cable on the deck depends on the angle between the horizontal and the cable: the lower the angle, the higher the horizontal force. As shown in Figure 25, the horizontal force exerted by one cable increases almost linearly with the distance from the pylons. This effect is true only for one given layout of the cable (fan, harp, mixed configuration). However, since it is preferable to increase the span without excessively increasing the height of the pylon, this angle is likely to decrease and the horizontal force to increase considerably. Even if such a strength requirement for the deck could be obtained using high performance materials like high performance concrete or steel, spanning a long distance with a cable-stayed bridge is ineffective.
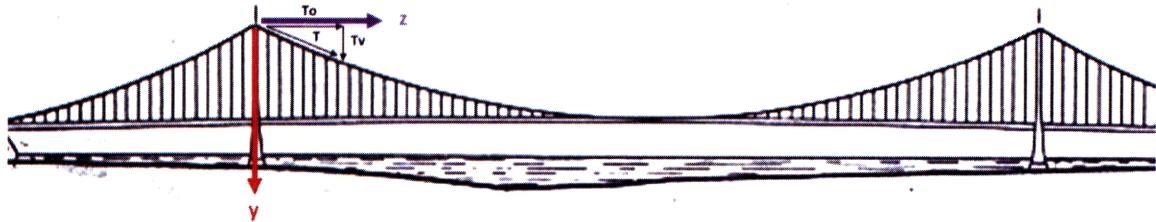
Figure 25: Maximum force exerted on the deck per cable

3.3 Suspension Bridges

3.3.1 Basic Analysis of the Main Cable – Contribution of Tensile Strength

The notations used are the following:

L	Length of the main span
h	Sag at middle span
z	Horizontal distance from the towers (cf. Figure 26)
y	Vertical distance from the anchorage point of the main cable
T	Tension of the main cable at the tower
T_v	Vertical component of the main cable at the tower
T_o	Horizontal component of the main cable at the tower
q	Unit weight per unit length, $q = \gamma A$ with:

	γ	Specific weight of the bridge
	A	Cross section of the deck

Figure 26: A classic suspension bridge
(adapted from Sequana Normandie [50])

Neglecting the cable weight with respect to the bridge weight is a standard practice to obtain the equation of the cable. It is still valid for a very long span, given the high specific strength of carbon nanotube cable. It is also assumed that the bridge is perfectly symmetric: the side spans are half the size of the main span.

The cable equation over the main span is given by [41]:

$$\frac{d^2y}{dz^2} = -\frac{q}{T_0} \tag{3.1}$$

Knowing the boundary conditions, the cable shape is derived:

$$y(z) = \frac{qL^2}{2T_0}\left(\frac{z}{L} - \frac{z^2}{L^2}\right) = \frac{h}{4}\left(\frac{z}{L} - \frac{z^2}{L^2}\right) \qquad (3.2)$$

with

$$h = y\left(\frac{L}{2}\right) = \frac{qL^2}{8T_0} \qquad (3.3)$$

The cable slope α at the tower is given by:

$$\tan(\alpha) = \frac{dy}{dz}(0) = \frac{qL}{2T_0} = 4\frac{h}{L} \qquad (3.4)$$

The compression on the tower, exerted per one set of cable is

$$T_v = q\frac{L}{2} \qquad (3.5)$$

so the axial force in the cable is given by:

$$T = \frac{T_v}{\sin(\alpha)} = \frac{T_0}{\cos(\alpha)} = \frac{qL^2}{8h\,\cos(\alpha)} \qquad (3.6)$$

This force cannot exceed

$$T_c = \sigma_c A_c \qquad (3.7)$$

with σ_c being the maximum allowable stress of the cable, and A_c its cross-section.

Then, the maximum limit span is obtained (calculation details are given in Appendix C):

$$L_{max} = h\sqrt{8\left(\sqrt{1 + \frac{\sigma_c^2 A_c^2}{\gamma^2 A^2 h^2}} - 1\right)} \qquad (3.8)$$

When h is small with respect to L_{max}, the equation becomes:

$$L_{max} \simeq \sqrt{\frac{8h\sigma_c A_c}{\gamma A}} = \sqrt{\frac{8h\sigma_c A_c}{q}} \qquad (3.9)$$

35

which gives the relationship between the maximum span and the allowable stress in the cable.

3.3.2 Basic Analysis of the Main Cable – Contribution of Stiffness

In this section, the influence of the stiffness on the deflection of the main cable (also called the hanging cable) is studied. The change in sag is computed when the full live load is applied to the bridge.

Between the towers, under the dead load, the length of the parabolic cable is given by:

$$l = 2 * \int_0^{\frac{L}{2}} \sqrt{1 + \left(\frac{dy}{dz}\right)^2} \, dz \qquad (3.10)$$

At a distance z from the tower, the strain in the cable is given by:

$$\text{strain}(z) = \frac{T(z)}{A_c E} \qquad (3.11)$$

where E is the Young's modulus of the cable, and $T(z)$ is the tension in the cable at the section considered. Assuming a uniform live load w is applied (the suspender ropes are supposed closely spaced, with respect to the length of the span), the equation of the tension is

$$T(z) = T \times cos\big(\alpha(z) - \alpha(0)\big) - qz \times sin(\alpha(z)) \qquad (3.12)$$

where s is the distance between two vertical stays, and α is the angle between the horizontal and the cable:

$$\alpha(z) = atan\left(\frac{dy(z)}{dz}\right) \qquad (3.13)$$

Then, noting (3.10), the new length of the cable under the live load is derived:

$$l_e = 2 * \int_0^{\frac{L}{2}} \sqrt{1 + \left(\frac{dy}{dz}\right)^2} \left(1 + \text{strain}(z)\right) dz \qquad (3.14)$$

Using (3.2) and (3.10), h is increased until l equals l_e. The corresponding h is h_e, the new sag.

The extension of the suspender ropes has few consequences, since they have a short length at the middle of the main span. Indeed, the sag is almost equal to the length of the tower above the roadway.

Another criterion involved in the deflection of the center span is the deflection of the towers. If the maximum longitudinal deflection of one tower towards the center of the bridge is given by δ_l, the deflection of the towers can be modeled as if the main cables measured $l_e + 2 \times \delta_l$ instead of l_e. Even if it is not exact because the cables are allowed to slip on the saddles, this additional length includes the other effects contributing to the deflection, for example, the effect of temperature. Once again, using (3.2) and (3.10), h is increased until l equals $l_e + 2 \times \delta_l$. The corresponding h is h_t, the total sag. Eventually, the final deflection ratio is

$$\delta_s = \frac{h_t - h_{\text{initial}}}{L} \qquad (3.15)$$

which has to be less than the allowable deflection.

3.3.3 Case Study: the Golden Gate Bridge

As was done previously for the cable-stayed bridge, the advantages of high performance carbon nanotube cable will be assessed, using the example of the Golden Gate Bridge (Figure 27). The longest bridge in the world from 1934 to 1964, the Golden Gate Bridge is very much appreciated by Americans, and it was elected the fifth on the list of *America's Favourite Architecture* in 2007 [42]. With its main span of 1,280 m, it is not now the longest bridge in the world (Akashi-Kaikyō Bridge, Japan – main span: 1,991 m), nor the longest American bridge (Verrazano-Narrows Bridge, NYC – main span: 1,298 m), but the Golden Gate Bridge might technically have the ability to reach an even longer span if its main cables alone were replaced.

The purpose of this study is to keep virtually all the original properties of this bridge: the cross section of the deck, linear dead and live load, spacing and section of suspender ropes, as well as allowed deflection ratio. The two main cables will be replaced by a carbon nanotube cable with the same diameter, and the towers will have the same height. They are assumed only to be reinforced in order to support the additional vertical load implied by the span extension.

Figure 27: The Golden Gate Bridge, San Francisco

(courtesy of Rich Niewiroski Jr.)

3.3.3.1 Data and Methodology

The following construction data are used [43; 44]:

Length of main span	1,280 m
Height of tower above roadway	152 m
Cable sag	143 m
Effective main cable diameter[2]	0.88 m
Effective main cable section[2]	0.60 m^2
Main cable tensile strength	1,517 MPa
Main cable Young's modulus	200,000 MPa
Safety Factor	2.7
Live load	58,450 N/m
Dead load	311,240 N/m
Longitudinal deflection of the tower (channelward)	0.46 m
Maximum downward deflection, at center span	3.3 m
Allowed deflection ratio (middle of the main span)[2]	1/388

To simplify, it is assumed that the bridge is symmetrical and that the side spans are half the length of the main span. It is also assumed that the tower is designed to have the same maximum longitudinal deflection channelward (0.46 m) for all span lengths. For each scenario, the Strength Based Design span will be computed using equation (3.14), and the Motion Based Design span will be computed iterating (3.10) to (3.15), until the maximum deflection allowable is obtained.

---

[2] Estimated by the author from the data

39

3.3.3.2 Results and Discussion

As shown in Table 4, by "simply" replacing the main cables with carbon nanotube cables, the main span can be considerably increased: +9.0% for the "pessimistic" scenario up to 79.2% for the "very optimistic" scenario. As for the cable-stayed bridge, the increase in stiffness is of major importance, and the span limit is often due to deflection requirements (except for the "high stiffness" scenario). It must be noted that a cable with the same diameter was used. If a cable having the same linear density had been used, the reachable spans would have been much longer, since the density of nanotubes is very low (approximately 1.3 g/cm^3) compared to steel (7.8 g/cm^3). The height of the tower can also be increased. If the height of the tower were equal to the Akashi-Kaikyō Bridge's tower (298 m), the reachable span would be 3,370 m for the "very optimistic scenario."

Table 4: Maximum spans reachable for the Golden Gate Bridge

Scenarios	Final Choice		SBD	MBD						
	L_{max} (m)	Increase in span	$L_{max\,SBD}$ (m)	$L_{max\,MBD}$ (m)	Initial length of the cable (m)	Additional length, due to the live load strain (m)	Additional length, due to deflection of the towers (m)	Final length of the cable (m)	Final deflection (m)	Deflection ratio
Reference $E = 200$ GPa $\sigma = 1.517$ GPa	1,280.00		1,280.00	1,280.00	1,321.41	1.14	0.92	1,323.47	3.30	1/388
Pessimistic $E = 250$ GPa $\sigma = 2$ GPa	1,395.00	+9.0%	1,469.71	1,395.00	1,433.16	0.98	0.92	1,435.06	3.59	1/388
High Stiffness $E = 500$ GPa $\sigma = 2$ GPa	1,469.71	+14.8%	1,469.71	1,795.00	1,824.93	1.02	0.92	1,826.87	4.62	1/388
High Strength $E = 250$ GPa $\sigma = 10$ GPa	1,395.00	+9.0%	3,286.38	1,395.00	1,433.16	0.98	0.92	1,435.06	3.59	1/388
Optimistic $E = 500$ GPa $\sigma = 10$ GPa	1,795.00	+40.2%	3,286.38	1,795.00	1,824.93	1.02	0.92	1,826.87	4.62	1/388
Very Optimistic $E = 1,000$ GPa $\sigma = 20$ GPa	2,294.00	+79.2%	4,647.64	2,294.00	2,317.55	1.05	0.92	2,319.52	5.91	1/388

40

In addition, replacing the suspender ropes with carbon nanotube ropes, and stiffening the towers would reduce the additional 0.92 m length, and would also improve the results. However, other parameters could reduce these theoretical spans, particularly dynamics considerations.

3.4 Dynamic Instabilities

Long span bridges are very sensitive to dynamic instabilities, particularly those caused by the wind. The first wind effect that has to be considered is the mean wind loading. It is characterized by a quasi-static load coming from the wind flow past the bridge. This load can produce horizontal, vertical or torsional forces. The amplitude of these forces can be calculated using the following formula [45]:

$$F = \frac{1}{2}\rho V^2 CA$$

where ρ is the air density, V is the mean wind velocity, C is the drag coefficient in the considered direction, and A is the exposed area. Consequently, decks with a low drag factor should be used, for example, streamlined box girders, which can reach drag coefficient as low as 0.025, a value ten times smaller than an open truss type stiffening girder [45].

Another additional effect is buffeting. These random turbulent fluctuations can produce dynamic responses if they excite the structure with a frequency close to the natural frequencies (vertical, lateral, torsional) of the deck. The main factors are the intensity of the wind and its distribution over the deck, the geometry of the deck, and the natural frequencies of the structure [45].

The third effect is vortex shedding. When the air flow meets the tower or the deck, flow separation occurs and results in vortices that shed alternatively on both sides. Therefore, a difference in pressure is created and the structure will tend to move toward the low-pressure zone, resulting in a periodic excitation, the frequency of which is [46]

$$f_s = S_t \frac{V}{D}$$

where S_t is the Strouhal number, V is the mean wind velocity, and D is the across wind width.

All these effects result in aerodynamics instability phenomena, which are caused by interaction among the loads applied, the mechanical properties of the deck, its deflections, and their resultant effects on the surrounding airflow. These instabilities can be a static torsional divergence, an instability in transverse bending (galloping), an instability in torsion (stall flutter), or an instability in coupled torsion and bending [45]. They can lead to the destruction of the bridge, as in the well known case of the Tacoma Bridge [47]. Therefore, a proper design and a wind tunnel testing must be carried out. An empirical formula gives the expression of the critical wind speed for classical flutters [45]:
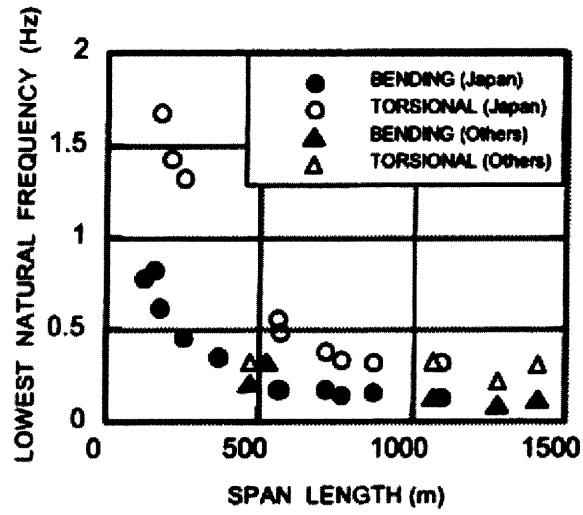
$$V_f = 4f_T B \left(1 - \frac{f_B}{f_T}\right) \sqrt{\frac{mr}{\rho B^3}}$$

where $f_{T/B}$ are the structure natural frequencies in torsion/bending, B is the width of the cross section, m is the mass per unit length of the structure, r is the polar moment of inertia of the bridge cross section, and ρ is the air density. For very long span bridges, the fundamental frequencies decrease (as shown in Figure 28), and the critical wind speed can become very low. Indeed,

$$f_{T/B} \propto \frac{\sqrt{EI}}{L^2}$$

so the bending and torsional rigidities of the deck, as well as its aerodynamics, have to be increased.

Another possibility to increase the overall stiffness of the bridge is to introduce additional cables parallel to the main cables, and attached to the towers as in a case of a cable-stayed bridge. These cables would be parallel to the main cables, above, but also below the deck. They could also be transversal to the main cable, adding lateral stiffness, and leading to a "spider's cobweb bridge" [48].

Figure 28: The lowest natural frequency vs. span length in suspension bridges
(Yamaguchi and Fujino [51])

Ideally, if the rigidities could be substantially increased by these additional strands, the design would no longer be governed by the displacements, and the Strength Based Design maximum spans given in Section 3.3.2 could be reached. Consequently, for the Golden Gate Bridge, the increase in span would be increased by 156% ("optimistic" scenario), or 263% ("very optimistic" scenario). Applied to the Akashi-Kaikyō Bridge, the "very optimistic" scenario would give a main span of 7,227 m.

Conclusion

In this thesis, it was shown that using 100 nanometers molecules to span 1,000 meters and more requires advanced research at every level.

At the nanoscale, carbon nanotubes have demonstrated extraordinary mechanical properties. Many efforts are being made to produce in industrial quantities carbon nanotubes having a quasi-perfect structure, length, diameter, number of walls, and chirality.

Making a fiber out of these nanotubes is a critical process in which the mechanical properties of nanotubes have to be transferred as efficiently as possible to the fiber. Currently, there are many results, and it is extremely difficult to predict the Young's modulus and the tensile strength of such a cable. As a result, in order to make projections, it was decided to assume different scenarios concerning these mechanical properties and to use them to evaluate the benefit in spanning long distances.

Cable-stayed bridges do not take full advantage of high performances cables. Indeed, theses bridges are intrinsically inadequate for long spans, because of the tremendous compression forces acting on the deck independently of the cables used. Nonetheless, the benefit of strong cables could be aesthetics, with the possibility to use slender cables and to increase the cable spacing.

Suspension bridges are the cable-stayed structures that could take the greatest advantage of carbon nanotube cables. However, even with their very high stiffness, spanning long distances will not be possible without additional mechanisms to reduce deflections and dynamic instabilities. Once these mechanisms are developed, it will be possible to design bridges spanning over five kilometers.

Appendix A: Full Code of the MATLAB® Program

```matlab
function [samplelv2 samplelv3 samplelv4 samplelv5 samplelv6 samplelv7]
= CNT_cable_strength()
%    Nanotube-Based Cable Strength Calculation
%    By Stephane Damolini
%    May 2009
clc; clf; clear all; tic;
global ii c cmax pcti ii jj delta_s0...
       lv1 lv2 lv3 lv4 lv5 lv6 s0 k0...
       ns2 ns3 ns4 ns5 ns6 ns7 pcti0...
       samplelv2 samplelv3 samplelv4...
       samplelv5 samplelv6 samplelv7
s0=34000;        %tensile strength use as base for Weibell statistic
k0=2.7;          %parameter of the Weibell statistic
ii=27;           %length of a base pattern
jj=373;          %width of a base pattern
delta_s0=1000;   %increment of tensile strength
ns2=1;           %Sampling size of level 1 used for level 2
ns3=10;          %Sampling size of level 2 used for level 3
ns4=10;          %Sampling size of level 3 used for level 4
ns5=10;          %Sampling size of level 4 used for level 5
ns6=5;           %Sampling size of level 5 used for level 6
ns7=5;           %Sampling size of level 6 used for level 7
samplelv2=zeros(ns2,1); samplelv3=zeros(ns3,1);
samplelv4=zeros(ns4,1); samplelv5=zeros(ns5,1);
samplelv6=zeros(ns6,1); samplelv7=zeros(ns6,1);
c=0;             %counter of progression
cmax=...         %total number of operations
    ii*jj*(1+ns2+ns3+ns4+ns5+ns6+ns7);
pcti=0;
pcti0=5;         %pourcentage increment for the counter
%First iteration level:
lv1='CptStrength(max_stress_level_1(ii,jj))';
%Second iteration level:
samplelv2=generate(ns2,lv1)
lv2='CptStrength(max_stress_level_n(ii,jj,samplelv2))';
%Third iteration level:
samplelv3=generate(ns3,lv2)
lv3='CptStrength(max_stress_level_n(ii,jj,samplelv3))';
%Fourth iteration level:
samplelv4=generate(ns4,lv3)
lv4='CptStrength(max_stress_level_n(ii,jj,samplelv4))';
%Fifth iteration level:
samplelv5=generate(ns5,lv4)
lv5='CptStrength(max_stress_level_n(ii,jj,samplelv5))';
%Sixth iteration level:
samplelv6=generate(ns6,lv5)
lv6='CptStrength(max_stress_level_n(ii,jj,samplelv6))';
%Seventh iteration level and display:
samplelv7=generate(ns7,lv6);
ans=CptStrength(max_stress_level_n(ii,jj,samplelv6));
disp(sprintf('\nThe final strength is %g Mpa.\n',ans))
toc;
close;
```

```
function s = CptStrength(max_stress)
global delta_s0
[m,n]=size(max_stress);
toredib=0;
cur_stress=zeros(m,n);
state=ones(m,n);
s=0;
s0=900;
remaining=1;
first_loop=1;
delta_s=0;
while 1
    if remaining==0; break; end
    s=s+delta_s;
    if first_loop==1
        delta_s=s0;
        s=s0;
    end
    for i=1:m
        remaining=0;
        for l=1:n
            remaining=remaining+state(i,l);
        end
        for j=1:n
            if state(i,j)==1
                cur_stress(i,j)=cur_stress(i,j)+delta_s*n/remaining;
            end
        end
        redis=0;
        while redis >= 0
            redis=-1;
            for p=1:n
                if cur_stress(i,p)>max_stress(i,p);
                    state(i,p)=0;
                    toredib=toredib+cur_stress(i,p);
                    cur_stress(i,p)=0;
                    redis = redis+1;
                end
            end
            if redis>=0
                remaining=0;
                for l=1:n
                    remaining=remaining+state(i,l);
                end
                if remaining==0;
                    break;
                else
                    s_add=toredib/remaining;
                    toredib=0;
                    for kk=1:n
                        if state(i,kk) == 1
                            cur_stress(i,kk)=cur_stress(i,kk)+s_add;
                        end
                    end
                end
            end
        end
    end
```

```matlab
            if remaining==0; break; end
        end
        if first_loop==1
            delta_s=delta_s0;
            first_loop=0;
        end;
    end
s=s-delta_s;
close;
```

```matlab
function g = generate(s,v)
global ii jj ns lv1 lv2 lv3 lv4 lv5 lv6 lv7...
    ns2 ns3 ns4 ns5 ns6 ns7...
    samplelv2 samplelv3 samplelv4...
    samplelv5 samplelv6 samplelv7
%s: size of sampling
%v: value of one sample
for i=1:s;
    g(i,1)=eval(v);
end
close;
```

```matlab
function max_stress_level_1 = max_stress_level_1 (m,n)
global s0 k0 ii jj ns lv1 lv2 lv3 lv4 lv5 lv6 lv7
for i=1:m
    for j=1:n
        max_stress_level_1(i,j)=(s0*(-log(rand(1)))^(1/k0));
        %counter;    %delete the '%' to enable counter
    end
end
max_stress_level_1;
close;
```

```matlab
function max_stress_level_n = max_stress_level_n (m,n,sample)
global ii jj ns lv1 lv2 lv3 lv4 lv5 lv6 lv7
ss=size(sample);
k=randint(ii,jj,[1 ss(1)]);
for i=1:m
    for j=1:n
        max_stress_level_n(i,j)=sample(k(i,j));
        %counter;    %delete the '%' to enable counter
    end
end
close;
```

```matlab
function [] = counter
global c cc pcti pcti0 cmax
c=c+1;
cc=c/cmax*100;
if cc>pcti disp(sprintf('Calculation in progress... [%g%%]', pcti))
    pcti=pcti+pcti0;
end
close
```

Appendix B: Calculation Details - Cable-Stayed Bridge

Data:

Young's modulus of cables	E=	2.000E+11	N/m3
Density of cables	γ=	7.36E+04	N/m3
Length of span	L=	114.3	m
Height of mast above deck	H=	54.0	m
Height of the deck above ground	h=	19.0	m
Young's modulus of deck	Ed=	2.00E+11	N/m3
Inertia of deck	Id=	0.333333333	m4
Total linear load on deck	w=	8.759E+04	N/m
Live load on deck	wl=	1.460E+04	N/m
Dead load on deck	wd=	7.300E+04	N/m
Weight of a single span	ps=	8.900E+05	N
Max stress allowable	σall=	1.50E+09	Pa
Deflection ratio allowed	δ=	0.00125	
Safety factor for the cables	sf=	2.5	

Cable spacing	s =	12.192	m	=	45	ft

Cable #	x (horizontal distance) (m)	y (cable's anchorage height from deck) (m)	Length of the cable (m)	Length of the cable (ft)	Angle btw cable and horizontal (degres)	Cable area [Strength based design] (m²)	Effective Young's Modulus of câbles (Pa)	Cable Area [Displacement based design] (m²)	Section driven by
1	12.19	28.66	31.14	102.17	66.95	3.869E-04	2.000E+11	1.145E-04	Strength
2	24.38	33.35	41.31	135.53	53.82	4.410E-04	2.000E+11	1.975E-04	Strength
3	36.58	36.94	51.99	170.56	45.29	5.009E-04	2.000E+11	3.206E-04	Strength
4	48.77	39.98	63.06	206.89	39.34	5.615E-04	2.000E+11	4.887E-04	Strength
5	60.96	42.65	74.40	244.09	34.98	6.210E-04	1.999E+11	7.053E-04	Displacement
6	73.15	45.07	85.92	281.89	31.64	6.787E-04	1.999E+11	9.734E-04	Displacement
7	85.34	47.29	97.57	320.11	28.99	7.345E-04	1.996E+11	1.296E-03	Displacement
8	97.54	49.36	109.31	358.64	26.84	7.884E-04	1.992E+11	1.677E-03	Displacement
9	109.73	51.30	121.13	397.40	25.06	8.405E-04	1.982E+11	2.122E-03	Displacement
10	121.92	53.14	133.00	436.34	23.55	8.910E-04	1.965E+11	2.641E-03	Displacement

Cable #	Cable area needed with safety factor (m²)	Cable diameter needed (cm)	Cable diameter needed (in)	Cable diameter choosen (cm)	Cable diameter choosen (in)	Final cable section (in²)	Final cable section (ft²)
1	9.672E-04	3.51	1.38	3.81	1.50	1.77	1.23E-02
2	1.103E-03	3.75	1.48	3.81	1.50	1.77	1.23E-02
3	1.252E-03	3.99	1.57	4.445	1.75	2.41	1.67E-02
4	1.404E-03	4.23	1.66	4.445	1.75	2.41	1.67E-02
5	1.763E-03	4.74	1.87	5.08	2.00	3.14	2.18E-02
6	2.433E-03	5.57	2.19	5.715	2.25	3.98	2.76E-02
7	3.240E-03	6.42	2.53	6.985	2.75	5.94	4.12E-02
8	4.193E-03	7.31	2.88	7.62	3.00	7.07	4.91E-02
9	5.305E-03	8.22	3.24	8.255	3.25	8.30	5.76E-02
10	6.603E-03	9.17	3.61	9.525	3.75	11.04	7.67E-02

Appendix C: Limit Span for a Suspension Bridge

The Pythagorean Theorem gives: $T^2 - T_0^2 = T_v^2$

Replacing T_v by $T_v = q\frac{L}{2}$ and T_0 by $\frac{qL^2}{8H}$ (using (3.2)):

$$T^2 - \frac{q^2L^4}{64h^2} = \frac{q^2L^2}{4}$$

$$\Rightarrow T^2 = \frac{q^2}{4}\left(\frac{L^4}{16h^2} + L^2\right)$$

$$\Rightarrow T^2 = \frac{q^2}{4}\left(\left[\frac{L^2}{4h} + 2h\right]^2 - 4h^2\right)$$

$$\Rightarrow T^2 = \frac{q^2}{4}\left(\left[\frac{L^2}{8h^2} + 1\right]^2 4h^2 - 4h^2\right)$$

$$\Rightarrow T^2 = q^2h^2\left(\left[\frac{L^2}{8h^2} + 1\right]^2 - 1\right)$$

$$\Rightarrow \frac{T^2}{q^2h^2} + 1 = \left[\frac{L^2}{8h^2} + 1\right]^2$$

$$\Rightarrow \sqrt{\frac{T^2}{q^2h^2} + 1} = \frac{L^2}{8h^2} + 1$$

$$\Rightarrow \frac{L^2}{h^2} = 8\left(\sqrt{\frac{T^2}{q^2h^2} + 1} - 1\right)$$

$$\Rightarrow L = h\sqrt{8\left(\sqrt{\frac{T^2}{q^2h^2} + 1} - 1\right)}$$

$$\Rightarrow L_{max} = h \sqrt{8 \left(\sqrt{1 + \frac{\sigma_c^2 A_c^2}{\gamma^2 A^2 h^2}} - 1 \right)}$$

Works Cited

[1] Iijima, S. (1991). Helical microtubules of graphitic carbon. *Nature , 354*, 56-58.

[2] Treacy, M. M., Ebbesend, T. W., & Gibson, J. M. (1996). *Nature* (381), 678.

[3] Salvetat, J.-P., Briggs, G. A., Jean-Marc Bonnard, R. R., Kulik, A. J., Stockli, T., Burnham, N. A., et al. (1999). Elastic and Shear Moduli of Single-Walled Carbon Nanotube Ropes. *Phys. Rev. Lett. , 82* (5), 944-947.

[4] Yakobson, B., Brabec, C. J., & Bernholc, J. (1996). *Phys. Rev. Lett.* (76), 2511.

[5] Falvo, M. R., Clary, G. J., R. M. Taylor II, V. C., Brooks, F. P., Washburn, S., & Superfine, R. (1997). *Nature* (389), 582.

[6] Yu, M. F., Lourie, O., Dyer, M., Moloni, K., Kelly, T. F., & Ruoff, R. S. (2000). *Science , 287* (637).

[7] Collins, P. G., & Avouris, P. (2000). Nanotubes for Electronics. *Scientific American Magazine* .

[8] Li, F., Cheng, H. M., Bai, S., Su, G., & Dresselhaus, M. S. (2000). Tensile strength of single-walled carbon nanotubes directly measured from their macroscopic ropes. *Applied Physics Letters* , 3161-3163.

[9] Pugno, N. M., Bosia, F., & Carpinteri, A. (2008). Multiscale Stochastic Simulations for Tensile Testing of Nanotube-Based Macroscopic Cables. *Small* (8), 1044-1052.

[10] (n.d.). Retrieved from Nano Werk Web site: http://www.nanowerk.com/news/newsid=8336.php

[11] Miessler, G. L., & Tarr, D. A. (2004). *Inorganic Chemistry* (3rd ed.). Pearson Education International.

[12] (n.d.). Retrieved from Nanotechnology Now: http://www.nanotech-now.com/nanotube-buckyball-sites.htm

[13] Maria Letizia Terranova, V. S. (2006). *The World of Carbon Nanotubes: An Overview of CVD Growth Methodologies.* WILEY-VCH Verlag GmbH & Co. KGaA, Weinheim.

[14] Terrones, M. (2004). *Carbon nanotubes: synthesis and properties, electronic devices and other emerging applications.* Institute of Materials, Minerals and Mining and ASM International.

[15] Dupas, C., Houdy, P., & Lahmani, M. *Nanoscience.* Springer.

[16] Radushkevich, L., & Lukyanovich, V. (1952). O strukture ugleroda, obrazujucegosja pri termiceskom razlozenii okisi ugleroda na zeleznom kontakte. *Zurn Fisic Chim* (26), 88-95.

[17] Monthioux, M., & Kuznetsov, V. L. (2006). Who should be given the credit for the discovery of carbon nanotubes? *Elsevier* .

[18] Oberlin, A., Endo, M., & Koyama, T. (1976). *J. Cryst Growth* (32), 335-349.

[19] Baddour, C. E., & Briens, C. (2005). Carbon Nanotube Synthesis: A Review. *International Journal Of Chemical Reactor Engineering* .

[20] Journet, C., Maser, W. K., Bernier, P., Loiseau, A., Lamy de la Chapells, M., Lefrant, S., et al. (1997). *Large-scale production of single-walled carbon nanotubes by the electric-arc technique.*

[21] Grobert, N. (2007). *Carbon nanotubes - becoming clean.* Materials Today.

[22] M. Jones, W. M. *Extrinsic and intrinsic effects on the exited-state of single-walled carbon nanotubes.* Nano Letters.

[23] O'Connell, M. J. *Carbon Nanotubes - Properties and Applications.* Taylor & Francis.

[24] A. Thess, R. L. (1996). *Science* (273), 483-487.

[25] Kuo, T. F., Chi, C. C., & Lin, I. N. (2001). *Synthesis of Carbon Nanotubes by Laser Ablation of Graphites at Room Temperature.* The Japan Society of Applied Physics.

[26] Y. Zhang, S. I. (1999). *Formation of single-wall carbon nanotubes by laser ablation of fullerenes at low temperature.* American Institute of Physics.

[27] Dillon, A. C., Parilla, P. A., Alleman, J., & Heben, J. D. (2000). *Chem. Phys. Lett.* (316), 13-18.

[28] P. C. Eklund, B. K. (2002). *Nano Letters* (2), 561-566.

[29] Popov, V. N. (2004). Carbon nanotubes: properties and applications. *Materials Science and Engineering Reports , 43*, 61-102.

[30] Schützenberger, P. *Sur quelques faits relatifs à l'histoire du carbone.* 1890: Comptes rendus de l'Académie des sciences de Paris.

[31] Ray H. Baughman, A. A. (2002). Carbon Nanotubes—the Route Toward Application. *Sciencemag Vol 297* .

[32] (n.d.). Retrieved from DuPont Web site: http://www2.dupont.com/Kevlar/en_US/

[33] Chae, H. G., & Kumar, S. (2008). Making Strong Fibers. *Science , 319.*

[34] Koziol, K., Vilatela, J., Moisala, A., Motta, M., Cunniff, P., Sennett, M., et al. (2007). High-Performance Carbon Nanotube Fiber. *Science , 318*, 1892-1895.

[35] Kis, A., Csányi, G., Salvetat, J.-P., Lee, T.-N., Couteau, E., Kulik, A. J., et al. (2004). Reinforcement of single-walled carbon nanotube bundles by intertube bridging. *Nature Publishing Group* .

[36] Ericson, L. M., Fan, H., Peng, H., Davis, V. A., Zhou, W., Sulpizio, J., et al. (2004). *Science* (305), 1447.

[37] Pugno, N., & Ruoff, R. (2006). *J. Appl. Phys. , 99.*

[38] Zhu, H. W., Xu, C. L., Wu, D. H., Wei, B. Q., & Vajtai, R. (2002). Direct Synthesis of Long Single-Walled Carbon Nanotube Strands. *Science* (884).

[39] M.Pugno, N. On the strength of the carbon nanotube-based space elevator cable: from nanomechanics to megamechanics. *J. Phys.: Condens. Matter* (18).

[40] Boutin, N., Damolini, S., Potapova, S., & Tao, A. (2009). *Longfellow Bridge Replacement.* M.Eng Project, Massachusetts Institute of Technology, Departement of Civil and Environmental Engineering, Cambridge.

[41] Connor, J. J. (2008). *1.571 Structural Analysis and Control.* MIT, Civil and Environmental Engineering.

[42] (n.d.). Retrieved from America's Favorite Architecture Web site: http://www.favoritearchitecture.org/

[43] (n.d.). Retrieved from The Golden Gate Bridge Web site: http://goldengatebridge.org/research/factsGGBDesign.php

[44] Haight, R. Q., Billington, D. P., & Khazem, D. (1997). Cable Safety Factors for Four Suspension Bridges. *Journal of Bridge Engineering* .

[45] Ryall, M. J., Parke, G. R., & Harding, J. E. (2000). *The Manual of Bridge Engineering.* Thomas Telford.

[46] Strommen, E. (2006). *Theory of Bridge Aerodynamics.* Springer.

[47] *Tacoma Narrows Bridge Collapse "Gallopin' Gertie".* (n.d.). Retrieved from http://www.youtube.com/watch?v=j-zczJXSxnw

[48] Carpinteri, A., & Pugno, N. (2008). Super-bridges Suspended Over Carbon Nanotubes Cables. *Journal of Physics: Condensed Matter* .

[49] (n.d.). Retrieved from Northwestern University Web site: http://www.discovernano.northwestern.edu/whatis/Glossary/whatis/Glossary/n-r_glossary.htm

[50] (n.d.). Retrieved from Sequana Normandie Web site: http://www.sequana-normandie.com/images/pontsusp.jpg

[51] Yamaguchi, H., & Ito, M. Full-scale measurements and structural damping of cable-supported bridges. *Proc. of Int. Bridge Conf.* Hong Kong.

[52] *IBMC.* (n.d.). Retrieved from http://www-ibmc.u-strasbg.fr/ict/images/SWNT_MWNT.jpg

[53] Shandakov, Lolli, G., Resasco, D. E., Choi, M., Tománek, D., & Kauppinen, E. I. (2007). A novel hybrid carbon material. *Nature Nanotechnology, 2*, 156-161.

[54] Saito, R., Fujita, M., Dresselhaus, G., & Dresselhaus, M. S. (1992). Electronic structure of chiral graphene tubules. *Appl. Phys. Lett., 60* (18).

[55] (n.d.). Retrieved from MRSEC Web site: http://mrsec.wisc.edu/Edetc/nanoquest/carbon/images/3nanotubes.gif

[56] (n.d.). Retrieved from Research Institute for Technical Physics and Materials Science Web site: http://www.mfa.kfki.hu/int/nano/results/arc.html

[57] (n.d.). Retrieved from Laser Focus World Web site: http://www.laserfocusworld.com/articles/231725

[58] (n.d.). Retrieved from COECS Web site: http://coecs.ou.edu/Brian.P.Grady/images/nanotube.jpg

[59] (n.d.). Retrieved from Life Boat Foundation Web site: http://lifeboat.com/images/space.elevator.jpg

Biographical Note

2008-2009
MASSACHUSETTS INSTITUTE OF TECHNOLOGY (MIT)
Cambridge, MA

Master of Engineering
High Performance Structures
Department of Civil and Environmental Engineering

2006-2009
ECOLE SPECIALE DES TRAVAUX PUBLICS (ESTP)
Paris, France

Diplôme d'Ingénieur des Travaux Publics

2004-2006
CLASSES PREPARATOIRES JANSON DE SAILLY
Paris, France

Mathématiques Supérieures MPSI
Mathématiques Spéciales MP